

**Designing global climate and atmospheric chemistry simulations for 1 km and 10 km diameter asteroid impacts using the properties of ejecta from the K-Pg impact**

Owen B. Toon<sup>1</sup>, Charles Bardeen<sup>2</sup>, Rolando Garcia<sup>2</sup>

<sup>1</sup> Department of Atmospheric and Oceanic Science, Laboratory for Atmospheric and Space Physics, University of Colorado, Boulder

<sup>2</sup> National Center for Atmospheric Research, Boulder, Colorado

*Correspondence to:* O.B. Toon (toon@lasp.colorado.edu)

**Abstract.** About 66 million years ago an asteroid about 10 km in diameter struck the Yucatan Peninsula creating the Chicxulub crater. The crater has been dated and found to be coincident with the Cretaceous-Paleogene (K-Pg) mass extinction event, one of 6 great mass extinctions in the last 600 million years. This event precipitated one of the largest episodes of rapid climate change in Earth history, yet no modern three-dimensional climate calculations have simulated the event. Similarly, while there is an on-going effort to detect asteroids that might hit Earth and to develop methods to stop them, there have been no modern calculations of the sizes of asteroids whose impacts on land would cause devastating effects on Earth. Here we provide the information needed to initialize such calculations for the K-Pg impactor and for a 1 km diameter impactor.

There is considerable controversy about the details of the events that followed the Chicxulub impact. We proceed through the data record in the order of confidence that a climatically important material was present in the atmosphere. The climatic importance is roughly proportional to the optical depth of the material. Spherules with diameters of several hundred-microns are found globally in an abundance that would have produced an atmospheric layer with an optical depth around 20, yet their large sizes would only allow them to stay airborne for a few days. They were likely important for triggering global wildfires. Soot, probably from global or near-global wildfires, is found globally in an abundance that would have produced an optical depth near 100, which would effectively prevent sunlight from reaching the surface. Nanometer sized iron particles are also present globally. Theory suggests these particles might be remnants of the vaporized asteroid and target that initially remained as vapor rather than condensing on the hundred-micron spherules when they entered the atmosphere. If present in the greatest abundance allowed by theory, their optical depth would have exceeded 1000. Clastics may be present globally, but only the quartz fraction can be quantified since shock features can identify it. However, it is very difficult to determine the total abundance of clastics. We reconcile previous widely disparate estimates and suggest the clastics may have had an optical depth near 100. Sulfur is predicted to originate about equally from the impactor and from the Yucatan surface materials. By mass, sulfur is less than 10 percent of the observed mass of the spheres and estimated mass of nano-particles. Since the sulfur probably reacted on the surfaces of the soot, nano-particles, clastics and spheres, it is likely a minor component of the climate forcing; however, detailed studies of the conversion of sulfur gases to particles are needed to determine if sulfuric acid

aerosols dominated in late stages of the evolution of the atmospheric debris. Numerous gases, including CO<sub>2</sub>, SO<sub>2</sub> (or SO<sub>3</sub>), H<sub>2</sub>O, CO<sub>2</sub>, Cl, Br, and I, were likely injected into the upper atmosphere by the impact or the immediate effects of the impact such as fires across the planet. Their abundance might have increased relative to current ambient values by a significant fraction for CO<sub>2</sub>, and by factors of 100 to 1000 for the other gases.

For the 1 km impactor, nano-particles might have had an optical depth of 1.5 if the impact occurred on land. If the impactor struck a densely forested region, soot from the forest fires might have had an optical depth of 0.1. Only S and I would be expected to be perturbed significantly relative to ambient gas phase values. One kilometer asteroids impacting the ocean may inject seawater into the stratosphere as well as halogens that are dissolved in the seawater.

For each of the materials mentioned we provide initial abundances and injection altitudes. For particles we suggest initial size distributions and optical constants. We also suggest new observations that could be made to narrow the uncertainties about the particles and gases generated by large impacts.

**Keywords** Climate modeling; Initial conditions; Asteroid impacts; K-Pg extinction

## **1. Introduction and definitions**

About 66 million years ago an asteroid around 10 km in diameter hit the Earth near the present day Yucatan village of Chicxulub and created an immense crater whose age coincides with the Cretaceous-Paleogene (K-Pg) global mass extinction (Alvarez et al., 1980; Schulte et al., 2010; Renne et al., 2013). There is an enormous literature concerning this event and its aftermath. Surprisingly, however, there are very few papers about the changes in climate and atmospheric chemistry caused by the debris from the impact while it was in the atmosphere, and no studies based on modern three-dimensional climate models. Nevertheless, this event was almost certainly one of the largest and most dramatic short-term perturbations to climate and atmospheric chemistry in Earth history.

There is substantial evidence for many other impacts in Earth history as large or larger than that at Chicxulub, mostly in the Pre-Cambrian (e.g. Johnson and Melosh, 2012a; Glass and Simonson, 2012). There is also a growing effort to find asteroids smaller than the one that hit Chicxulub, but whose impact might have significant global effects, and to develop techniques to stop any that could hit the Earth. For example, as of November 17, 2015 NASA's Near Earth Object Program identifies 13,392 objects whose orbits pass near Earth. Among these objects, 878 have a diameter of about 1 km or larger, and 1640 have been identified as Potentially Hazardous Asteroids, which are asteroids that pass the Earth within about 5% of Earth's distance from the sun, and are larger than about 150 m diameter.

There is evidence for such smaller impacts in recent geologic history from craters, osmium variations in sea cores (Paquay et al., 2008), and spherule layers (Johnson and Melosh, 2012a; Glass and Simonson, 2012). For instance, a multi-kilometer object formed the Siberian Popigai crater in the Late Eocene and another multi-kilometer object

85 formed the Late Eocene Chesapeake Bay crater in the United States. Size estimates vary  
86 between techniques, but within a given technique the Popigai object is generally given a  
87 diameter half that of the Chicxulub object. Toon et al. (1997) point out that the  
88 environmental effects of impacts scale with the impactor energy, or cube of the diameter,  
89 not diameter (or crater size). The Popigai object likely had about 12% of the energy of  
90 the Chicxulub object. Surprisingly, except for collisions in the ocean (Pierazzo et al.,  
91 2010), climate models have not been used to determine the destruction that might be  
92 caused by objects near 1 km in diameter, a suggested lower limit to the size of an  
93 impactor that might do significant worldwide damage (e.g. Toon et al., 1997).

94 Here we describe the parameters that are needed to initialize three-dimensional climate  
95 and atmospheric chemistry models for the Chicxulub impact and for a 1-km diameter  
96 asteroid impact. Nearly every aspect of the K-Pg impact event is uncertain, and  
97 controversial. We will address some of these uncertainties and controversies and make  
98 recommendations for the initial conditions that seem most appropriate for a climate  
99 model, based upon the geological evidence. We will also suggest the properties of the  
100 initial impact debris from a 1 km diameter asteroid.

101 There are numerous observed and predicted components of the Chicxulub impact debris.  
102 The distal debris layer, defined to be the debris that is more than 4000 km removed from  
103 the impact site, is thought to contain material that remained in the atmosphere long  
104 enough to be globally distributed. This distal layer, sometimes called the fireball layer or  
105 the magic layer, is typically only a few mm thick (Smit, 1999). As discussed below, the  
106 layer includes 200  $\mu\text{m}$ -sized spherules, 50  $\mu\text{m}$ -sized shocked quartz grains, 0.1- $\mu\text{m}$ -sized  
107 soot and a 20 nm-sized iron-rich material.

108 We discuss each of the components of the distal layer in detail below. In brief, we find  
109 the following: The large spherules are not likely to be of importance to the climate  
110 because they would have been removed from the atmosphere in only a few days.  
111 However, they may have initiated global wildfires. The shocked quartz grains, one of the  
112 definitive pieces of evidence for an impact origin as opposed to volcanic origin of the  
113 debris layer, is likely only a small fraction of the clastic debris. It is difficult to identify  
114 the rest of the minerals produced by crushing because there is material in the layer that  
115 might have been produced long after the impact by erosion and chemical alteration of the  
116 large spheres or from the ambient environment. One major controversy surrounding the  
117 clastic material is the fraction that is submicron-sized. Particles larger than a micron will  
118 not remain in the atmosphere very long and, therefore, are less likely to affect climate.  
119 Unfortunately, the sub- $\mu\text{m}$  portion of the clastics in the distal layer, which might linger in  
120 the atmosphere for a year or more, has not been directly measured. Our estimate of the  
121 mass of submicron-sized clastics suggest that it could have had a very high large optical  
122 depth that would be capable of modifying the climate significantly. Nevertheless,  
123 submicron clastics are only of modest climatic importance relative to the light absorbing  
124 soot and possibly the iron rich nm-scale debris. Submicron soot is observed in the global  
125 distal layer in such quantity that it would have had a very great impact on the climate  
126 when it was suspended in the atmosphere. The major controversy surrounding the soot is  
127 whether it originated from forest fires, or from hydrocarbons at the impact site. The  
128 origin of the soot, however, is of secondary importance with regard to its effect on  
129 climate. Since the soot layer overlaps the iridium layer in the distal debris it had to have

130 been created within a year or two of the impact, based on the removal time of small  
131 particles from the atmosphere (and ocean), and could not have been the result of fires  
132 long after the impact. The fireball layer is often colored red and contains abundant iron.  
133 Some of the iron has been identified as part of a 20 nm-sized particle phase, possibly  
134 representing a portion of the recondensed vaporized impactor and target. However,  
135 relatively little work has been done on this material. Its abundance has not been  
136 measured, but theoretical work suggests its mass could have been comparable to that of  
137 the impactor. Therefore, the nm-sized particles could have been of great importance to  
138 the climate. Each of the materials just described is present in the distal layer, and their  
139 impacts on the atmosphere were likely additive.

140 There are several other possible components of the distal layer that have not been clearly  
141 identified and studied as part of the impact debris, which we discuss below. Water,  
142 carbon, sulfur, chlorine, bromine, and iodine were likely present in significant quantities  
143 in the atmosphere after the impact. The Chicxulub impact occurred in the sea with depths  
144 possibly ranging up to 1 km. The target sediments and the asteroid probably also  
145 contained significant amounts of water. Water is an important greenhouse gas, and could  
146 condense to form rain, which might have removed materials from the stratosphere.  
147 Carbon is present in seawater, in many asteroids and in sediments. Injections as carbon  
148 dioxide or methane might have led to an increased greenhouse effect. Sulfur is widely  
149 distributed in the ambient environment, and is water-soluble. Therefore, it is difficult to  
150 identify extraterrestrial sulfur in the debris layer. However, the impact site contains a lot  
151 of sulfur, and asteroids also contain significant amounts of sulfur. Sulfur is noteworthy  
152 because it is known to produce atmospheric particulates in today's atmosphere that alter  
153 the climate. Chlorine, bromine and iodine can destroy ozone, and their effectiveness as  
154 catalysts is enhanced by heterogeneous reactions on sulfuric acid aerosols.

155 In addition to the mm-thick distal layer, there is an intermediate region ranging from  
156 2,500-4,000 km from the impact site with a debris layer that is several cm thick (Smit,  
157 1999). This layer contains microtektites (molten rock deformed by passage through the  
158 air), shocked quartz, as well as clastics such as pulverized and shocked carbonates. Most  
159 of this layer originated from the target material in the Yucatan. It is of interest because,  
160 like the debris clouds from explosive volcanic eruptions, components of this material  
161 may have escaped from the region near the impact site to become part of the global debris  
162 layer.

163 Properties of each of these materials need to be known in order to model their effects on  
164 the climate and atmospheric chemistry realistically. These properties include the altitude  
165 of injection, the size of the injected particles, the mass of injected particles or gases, the  
166 density of the particles, and the optical properties of the injected particles and gases. Our  
167 best estimates for these properties for the K-Pg impact are summarized in Table 1 for  
168 particles and Table 2 for gases, and discussed for each material in Section 2. Tables 3  
169 and 4 provide an extrapolation of these properties for an impact of a 1 km sized object.

170 While the mass of the injected material is useful as an input parameter to a model, the  
171 optical depth of the particles is needed to quantify their impact on the atmospheric  
172 radiation field and, therefore, on the climate. Hence, optical depth is a useful quantity to  
173 compare the relative importance of the various materials to the climate. For a

monodisperse particle size distribution, the optical depth is given by  $\tau = \frac{3Mq_{\text{ext}}}{4\rho r}$ . Here  $M$

is the mass of particles in a column of air (for example,  $\text{g cm}^{-2}$ ),  $r$  is the radius of the particles,  $\rho$  is the density of the material composing the particles, and  $q_{\text{ext}}$  is the optical extinction efficiency at the wavelength of interest. The optical extinction efficiency is a function of the size of the particles relative to the wavelength of light of interest, and of the optical constants of the material. The optical extinction efficiency is computed accurately in climate models. However, a rough value of  $q_{\text{ext}}$  for particles larger than  $1 \mu\text{m}$ , is about 2 for visible wavelength light. We use this rough estimate for  $q_{\text{ext}}$  in Table 1 and Table 3 to calculate an optical depth for purposes of qualitatively comparing the importance of the various types of injected particles. We assume in the heuristic calculations of optical depth in Tables 1 and 3 that the particles have a radius of  $1 \mu\text{m}$  because smaller particles will quickly coagulate to a radius near  $1 \mu\text{m}$  given the large masses of injected material. Particles smaller than  $1 \mu\text{m}$  would lead to a larger optical depth than given in Tables 1 and 3.

Below we define the properties that are needed to perform climate or atmospheric chemistry simulations for each material that might be important.

## **2. Particulate Injections**

### **2.1 Large spherules**

#### **2.1.1 Large spherules from the Chicxulub impact**

The most evident component of the distal and regional debris layers is spherical particles, some of which are large enough to be seen with the naked eye. Due to their spherical shape it is assumed that they are part of the melt debris from the impact or the condensed vapor from the impact (Johnson and Melosh, 2012b; 2014). The particles are not thought to have melted on reentry into the atmosphere since debris launched above the atmosphere by the impact should not reach high enough velocities to melt when it reenters the atmosphere. According to Bohor and Glass (1995) there are two types of spherules, with differing composition and distribution. They identify Type 1 splash-form spherules (tektites or microtektites) that occur in the melt-ejecta (basal or lower) layer of the regional debris layer where it has a two-layered structure. These spherules are found as far from the Chicxulub site as Wyoming, but generally do not extend beyond about 4000 km away from Chicxulub. While the type 1 particles are derived from silicic rocks, they are also mixed with sulfur rich carbonates from the upper sediments in the Yucatan. The Type 1 spherules are poor in Ni and Ir, and the lower layer is poor in shocked quartz, consistent with their origin from the lower energy impact ejecta from the crater. Generally, the debris layer within about 4000 km of the crater is almost entirely composed of target material, rather than material from the impactor itself. Type 2 spherules, on the other hand, are found in the distal debris layer, and presumably formed primarily from the condensation of rock vapor from the impactor and target (O'Keefe and Ahrens, 1982; Johnson and Melosh, 2012b). There are sub-types of Type 2 spherules that correspond to varying composition of the original source material. Type 2 spherules occur in the upper layer in impact sites near Chicxulub, which merges into the fireball

layer at distal sites. The Type 2 spherules are rich in Ni and Ir, while the fireball layer is rich in shocked quartz.

The formation of the spherical particles may depend on two different processes. Melosh and Vickery (1991) describe one formation mechanism, probably occurring in less heavily shocked portions of the target, when molten material decompresses until it reaches a critical line at which it starts to boil. The gas drag from the rock vapor on the molten rock spheres then tears apart the molten material, just as water droplets break apart when they fall through air. The relative velocities of water drops in air and the melt in vapor are similar, as are the surface tensions. As a result melt droplets are similar in size to drizzle drops in light rain, near  $250\ \mu\text{m}$ . According to Johnson and Melosh (2012b) these spherical particles are most likely to be found within 4000 km of the impact site, and to be chemically related to the target material, and not to the impactor. Such materials are reported across North America as Type 1 spherules (Bohor et al., 1987), sometimes referred to as microtektites. Since these spherules are not global, they likely were not as relevant to climate as the Type 2 spherules.

Melt droplets can also form in heavily shocked parts of the impact debris as rock vapor condenses to form melt in the fireball, which rises thousands of km above the Earth's surface. These melt droplets form the Type 2 spherules. O'Keefe and Ahrens (1982) first modeled this process, and deduced that particles near a few hundred microns in size would form, as is observed. They also pointed out that the size of the spheres would be proportional to the size of the impactor. Johnson and Melosh (2012b) recently reconsidered this process for forming melt particles. They point out that the large spherules contain iridium (e.g., Smit, 1999), which is consistent with them being composed partially of the vaporized impactor. Their model of the formation and distribution of these particles suggests the particles have a size that varies spatially over the plume. Averaging over the simulated plume yields a mean size of  $217\ \mu\text{m}$  with a standard deviation of about  $47\ \mu\text{m}$  for a 10 km diameter impactor hitting at  $21\ \text{km s}^{-1}$ . From the two examples given by Johnson and Melosh (2012b) it appears that the standard deviation is consistently 22% of the mean radius for asteroids of different sizes. The initial values for the various properties of Type 2 spherules described above are summarized in Table 1 for the K-Pg impactor.

Smit (1999), who refers to the Type 2 spherules in the distal layer as microkrystites, estimated that these particles typically have a diameter near  $250\ \mu\text{m}$ , and a surface concentration of about 20,000 particles  $\text{cm}^{-2}$  over the Earth. Unfortunately, we are not aware of studies that measure the dispersion of the size distribution, or the spatial variation of the abundance of these particles. We assume that the particles have the density of CM2 asteroids, since Cr isotope ratios suggest that is the composition of the K-Pg impactor (Trinquier et al., 2006). Assuming this density,  $\sim 2.7\ \text{g cm}^{-3}$ , the mass of spherules per unit area of the Earth is about  $0.4\ \text{g cm}^{-2}$ , and the initial optical depth is about 20, as noted in Table 1. These spherules compose about half of the mass of the distal layer. We assume the particles were initially distributed uniformly around the globe, with the initial mixing ratio in the atmosphere varying only in altitude. Some theoretical studies, such as Kring and Durda (2002) and Morgan et al. (2013), suggest

that these particles were not uniformly deposited in latitude and longitude, but had focusing points such as the antipodes of the impact site. Unfortunately, we are not aware of quantitative data on the global distribution of the spherules. The study by Morgan et al. (2013) may also be more applicable to the Type 1 spherules since their numerical model does not produce vaporized material from the asteroid impact.

According to the simulations of Goldin and Melosh (2009), the in-falling spherical particles reached terminal fall velocity near 70km altitude, at which point they begin to behave like individual airborne particles. Kalasnikova et al. (2000) investigated incoming micrometeorites in the present atmosphere, which generally ablate near 85 km. Kalasnikova et al. (2000) find material entering from space stops in the atmosphere after it encounters a mass of air approximately equal to its own mass. Therefore, the altitude distribution is taken to be Gaussian, centered at 70 km and with a half-width of one atmospheric scale height (about 6.6 km based on the U.S. Standard Atmosphere). A scale height is chosen as the half width of the injection profile since it is a natural measure of the density of the atmosphere. Figure 1 illustrates the vertical injection profile of the spherules (green curve). As discussed below we expect several materials with origins similar to those of the spherules to be injected in this same altitude range, but others with origins unrelated to the impact generated plume, such as soot from fires, to be injected at lower altitudes.

The 70 km injection altitude refers to the level at which the large spherical particles reached terminal velocity. However, as is evident from the optical depth, many spherules entered through the same air mass. The column mass of the distal layer is  $\sim 1 \text{ g cm}^{-2}$  so the air pressure needs to about 1 hPa for the air mass above the altitude in question and the particle mass to be comparable. A pressure of 1hPa occurs at about 48 km. Therefore, if the entire distal layer mass is placed into a model above 48 km its mass mixing ratio will be greater than 1, and the atmosphere will be significantly out of hydrostatic balance. We are not aware of any simulations of the first few hours after the impact, but significant turbulence and mixing must have occurred as the atmosphere adjusted to the large mass imbalance. Model initialization should be checked to determine if the planned simulations start out of hydrostatic balance. If so, the injection altitude should be lowered below 70 km.

The energy release from the reentry of the large spherical particles into the atmosphere was likely responsible for setting most of the above ground terrestrial biosphere on fire. However, due to their size, the spherules could not have remained in the atmosphere for more than a few days. Hence they likely did not have a significant direct impact on the climate, but fell to Earth like a gentle rain.

### **2.1.2 Large spherules from a 1 km diameter asteroid impact**

Type 1 spherules, melt droplets, will form from impacts by 1 km diameter asteroids, and produce mm-sized particles in the ejecta curtain layer located near the crater (Johnson and Melosh, 2014). We do not expect an impact by a 1 km diameter asteroid to create a global layer of Type 2 spherules (Toon et al., 1996). Like O’Keefe and Ahrens (1982), Johnson and Melosh (2012b) conclude that the particle size will vary in proportion to the

impactor diameter and the impactor velocity. For a 1 km diameter impactor hitting the land at 20 km/s they suggest that the mean diameter of the spherical particles will be about 15  $\mu\text{m}$ , with somewhat larger sizes as the impact velocity increases to 30 km/s. Table 3 provides our assumed properties of the spherules from a hypothetical 1 km diameter impactor hitting the land. It is likely that spherules would not be distributed over all of the globe for the 1 km diameter impact. Johnson and Melosh (2012a) as well as Glass and Simonson (2012) report a spherule layer associated with the Popagai impact in the late Eocene which Johnson and Bowling (2014) suggest was global in extent. This layer contains spherules similar in size or even larger than those associated with the Chicxulub impact. However, this layer is only about 10% as thick as the distal layer from the Chicxulub impact. A 1 km impactor hitting the deep oceans may not produce a layer of spherules.

## **2.2 Soot**

### **2.2.1 Soot from the Chicxulub impact**

Spherical soot (also referred to as black carbon, or elemental carbon) particles were discovered in the boundary layer debris at sites including Denmark, Italy, Spain, Austria, Tunisia, Turkmenistan, the United States and New Zealand, among others by Wolbach et al. (1985; 1988; 1990a, 1990b). Soot was also found in anaerobic deep-sea cores from the mid-Pacific (Wolbach et al., 2003). Soot was apparently lost by oxidation in aerobic deep-water sites in the 66 million years since emplacement. There is debate about whether these particles originated from global wildfires, or from the impact itself (Belcher et al., 2003, 2004, 2005, 2009; Belcher, 2009; Harvey et al., 2008; Robertson et al., 2013a; Pierazzo and Artemieva, 2012; Premovic' 2012; Morgan et al., 2013; Kaiho et al., 2016). Robertson et al. (2013), Pierazzo and Artemieva (2012), Premovic' (2012) and Morgan et al. (2013) argue that it is implausible that there was enough carbon at the impact site to produce the amount of soot observed by Wolbach et al. (1988). This debate about the origin of the particles does not greatly affect the impact these particles would have had on the climate when they were suspended in the atmosphere. The particles are small and widely distributed. They are numerous and so must have produced a very large optical depth and, being composed of carbon, they would have been excellent absorbers of sunlight. Whether the soot particles originated from global fires and were deposited in the upper troposphere, or they originated at the impact site and were deposited in the mesosphere, the climate effect of the observed soot would have been very great. Some have suggested that the soot resulted from wildfires in dead and dying trees that occurred well after the impact. However, Wolbach et al. (1988; 1990b) show that soot and iridium are tightly correlated and collocated. Indeed, Wolbach et al. (1990b) suggest the soot and iridium may have coagulated in the atmosphere. The soot and iridium in the distal layer must have been deposited within a few years of the impact, since small particles will not stay in the air much longer. Therefore, any fires must have been very close in time to the impact, and were likely contemporaneous.

Wolbach et al. (1988) estimated the global mass of elemental carbon (including aciniform soot, charcoal and any unreactive aromatic kerogen) in the debris layer as  $7 \pm 4 \times 10^4$  Tg of C or equivalently  $13 \pm 7$  mg C  $\text{cm}^{-2}$  based on data from 5 sites. Wolbach et al. (1990b)

updated these mass determinations to  $5.6 \pm 1.5 \times 10^4$  Tg or  $11 \pm 3$  mg C cm<sup>-2</sup> based on data from 11 sites. This mass of elemental carbon would require that the bulk of the above ground biomass burned and was partially converted to elemental carbon with an efficiency of about 3%, assuming the biomass is 1.5 g C cm<sup>-2</sup> of above ground, dry organic mass per cm<sup>2</sup> over the land area of Earth. This biomass density is typical of current tropical forests. This inferred 3% emission factor is about 60 times greater than that suggested by Andreae and Merlet (2001) for current wildfires, but agrees with laboratory and other observations from burning wood under conditions consistent with mass fires (Crutzen et al., 1984; Turco et al., 1990). Mass fires are more intense than forest fires, and consume all the fuel available, possibly including that in the near surface soil. Ivany and Salawitch (1993) argued independently from oceanic carbon isotope ratios that at least 25% of the above ground biomass must have burned at the K-Pg boundary.

Wolbach et al. (1990b) distinguish several forms of elemental carbon. Aciniform carbon is composed of grape-like clusters of 0.01 to 0.1  $\mu$ m spherules. On average, this type of soot is 26.6% of the elemental carbon, yielding a global mass abundance of  $1.5 \times 10^4$  Tg of aciniform carbon. Charcoal is estimated at 3.3 to  $4.1 \times 10^4$  Tg, and unreactive kerogen at 0 to  $0.8 \times 10^4$  Tg. Wolbach et al. (2003) discuss a data set from the mid-Pacific that suggests aciniform soot is  $9 \times 10^3$  Tg, and charcoal is also  $9 \times 10^3$  Tg. Wolbach et al. directly measure the carbon content of their samples. The aciniform soot to charcoal ratio is determined by using an electron microscope to distinguish small and large particles.

There are several uncertainties in determining the amount of soot to use in a model. An upper limit of the amount injected into the stratosphere is  $7.1 \times 10^4$  Tg based on the upper error bar of the Wolbach et al. (1990b) elemental carbon values. An important assumption in this upper limit is that the larger particles found by Wolbach et al. (1990b), are either aggregates of smaller ones, or of the same general size as the aggregates of the smaller ones that occur after coagulation. A lower limit of  $1.1 \times 10^4$  Tg is obtained using the lower error bar of the elemental carbon from Wolbach et al. (1990b), and assuming 26.6% is aciniform soot. Alternatively, one could argue that this lower limit of aciniform soot should be injected into the stratosphere, along with  $3.3 \times 10^4$  Tg of charcoal using different size distributions. The most likely value of the aciniform soot in the stratosphere is  $1.5 \times 10^4$  Tg, and of elemental carbon  $5.6 \times 10^4$  Tg. We use these most likely values in Table 1.

Kaiho et al. (2016) argue that the soot came from burning hydrocarbons in the crater and that the total mass emitted was either  $5 \times 10^2$ ,  $15 \times 10^2$  or  $26 \times 10^2$  Tg. If we reduce these values by the author's factor of 2.6 to represent the stratospheric emissions, they are 0.4%, 1.0% and 1.7% of the globally distributed elemental carbon reported by Wolbach et al. (1990b).

Kaiho et al. (2016) measured several polycyclic aromatic hydrocarbons (PAHs) that are minor components of soot from one distal site in Caravaca, Spain, and another site at Beloc, Haiti that is about 700 km from the crater. Since the PAHs measured are minor constituents of soot Kaiho et al. (2016) need to use a large correction factor to determine the amount of soot. They first multiply by factors of 2, 5.9, or 10 to account for possible loss of PAH concentrations over time. They present no data to justify these factors. They

then multiply by  $3.3 \times 10^3$  citing this as the ratio of their measured PAHs to soot in diesel soot. No error bars were presented for this factor, and no values were given for the ratio in biomass soot. The origin of this correction factor is not evident in the cited reference. They then multiplied by another factor of 2.6 to represent the fraction of their soot estimate that they suspect reached the stratosphere. Their overall correction factors were therefore  $17 \times 10^3$ ,  $50 \times 10^3$ , and  $86 \times 10^3$ . Given these large correction factors, and the lack of information about their uncertainty, it is difficult to compare them with the direct determinations done by Wolbach et al. (1990b), which do not require any correction factors.

As noted in Table 1, the mass of soot found by Wolbach et al. (1988) would produce an optical depth near 100 if the particles coagulated to spheres with a radius of  $1 \mu\text{m}$  while they were in the atmosphere. Toon et al. (1997) pointed out that soot clouds with such a large optical depth would reduce light levels at the Earth's surface effectively to zero. The optical and chemical evolution of the particles once in the atmosphere may be influenced by the presence of liquid organics on the soot particles. Bare soot particles coagulate into chains and sheets, while particles that are coated by liquids may form balls. Chains, sheets, and coated balls have very different optical properties than do spheres (Wolf and Toon, 2010; Ackerman and Toon, 1981; Bond and Bergstrom, 2006; Mikhailov et al., 2006). Particulate organic matter can be absorbing, and soot coated with organics can have enhanced absorption relative to soot that is uncoated (Lack et al., 2012; Mikhailov et al., 2006). These fractal shapes, and organic coatings might not be preserved in samples in the distal layer since all the particles have been consolidated in a layer, and even in the current atmosphere the organics have short lifetimes due to rapid oxidation.

Wolbach et al. (1985) fit the size of the particles they observed, after exposing them to ultrasound to break up agglomerates, to a lognormal size distribution, described by

$$\frac{dN}{d \ln r} = \frac{N_t}{\ln \sigma \sqrt{2\pi}} \exp\left[-\left(\ln^2\left(\frac{r}{r_m}\right) / 2 \ln^2 \sigma\right)\right]. \quad (1)$$

Here  $r$  is the particle radius,  $N_t$  is the total number of particles per unit volume of air,  $r_m$  is the mode radius, and  $\sigma$  is the width of the distribution. Wolbach et al. (1985) find  $r_m = 0.11 \mu\text{m}$ , and  $\sigma = 1.6$  for the soot in the K-Pg boundary layer. We assume this distribution represents the initial sizes of the soot particles. The final size, which would be determined by coagulation while in the atmosphere, might not be preserved in the sediments, and loosely bound clumps of particles would have been destroyed by the ultrasound treatment of the samples.

The size distribution of soot from the K-Pg boundary is similar to that of smoke nearby present day biomass fires as indicated in Fig. 2 (e.g., Matichuk et al., 2008). This similarity in sizes is somewhat surprising because the present day smoke size distribution includes organic carbon, which is present in addition to the elemental carbon (soot). Generally, in wildfire smoke organic carbon has 5-10 times the mass of soot, so one might anticipate that the K-Pg soot would be about half the size of the present day smoke rather than of similar size since the organic coatings are no longer present, or were never

present, on the K-Pg soot. The organics might never have been present, because mass fires are very intense and tend to consume all the available fuel, which might include the organic coatings. Aggregation in the hot fires may have caused this slightly larger than expected size in the K-Pg sediments. Wolbach et al. (1985) suspended their samples in water and subjected them to ultrasound for 15 minutes in a failed attempt to completely break up agglomerates. This failure indicated that the remaining agglomerates might have been flame-welded. Therefore, the K-Pg size distribution from Wolbach et al. (1985) does not represent the monomers in the aggregate soot fractal structures. Rather the K-Pg size distributions represent a combination of monomers and aggregates that may have formed at high temperatures. Possibly the smallest sized particles measured by Wolbach et al. (1985), which have radii of 30-60 nm, represent the soot monomers. These are in the same general range as monomer sizes observed in soot from conventional fires (Bond and Bergstrom, 2006).

The injection altitude of the soot depends on its source. In a series of papers Belcher et al. (2003; 2004; 2005; 2009) and Belcher (2009) argue from multiple points of view that there were no global forest fires. Harvey et al. (2008) and Kaiho et al. (2016) argue that the soot originated from oil, coal and other organic deposits at the location of the impact. If correct, the soot might have been injected at high altitude along with the large spherules. Recently, Robertson et al. (2013a) reconsidered each of the arguments presented by Belcher et al. (2003; 2004; 2005; 2009) and Belcher (2009) and came to the conclusion that global wildfires did indeed occur. Pierazzo and Artemieva (2012), Premovic (2012), Morgan et al. (2013), as well as Robertson et al. (2013a) have independently argued that oil and other biomass in the crater is quantitatively insufficient to be the source of the soot. Therefore, we assume that the soot indeed originated from burning biomass distributed over the globe. The soot is clearly present in the distal layer material, and therefore was once in the atmosphere where it could cause significant changes to the climate.

Toon et al. (2007) have outlined the altitudes where one expects large mass fires to inject their smoke. Numerical simulations have shown that mass fires larger than about 5 km in diameter have smoke cloud tops well into the stratosphere. The smoke itself is distributed over a range of heights, however. The details of the injection profiles depend on the rate of fuel burning, the size of the fires, and the meteorological conditions among other factors. In addition, some smoke is quickly removed from the atmosphere by precipitation in pyro-cumulus. However, it is thought that over-seeding of the clouds by smoke prevents precipitation, and that only 20% or so of the smoke injected into the upper troposphere is promptly rained out (Toon et al., 2007). Smoke that is injected near the ground, on the other hand, will be removed by rainfall within days of weeks.

The K-Pg impact occurred at a time when average biomass density likely was higher than now. Following Small and Heikes (1988; their Figure 3f) and Pittock et al. (1989) one would expect smoke from large area fires burning in high biomass density areas to show a bi-modal smoke injection profile. The smoke at higher levels is injected in the pyro-cumulus and other regions with strong vertical motions. However, once the fires die-down smoke will be emitted in the boundary layer. There are also downdrafts, as well as

entrainment and mixing with the environment, that occur in all cumulus and these will carry some smoke into the boundary layer. We simulate this with injections whose vertical distributions are Gaussian functions centered at the tropopause and at the surface, as illustrated in Fig. 1. The injection at the tropopause (Eq. 2) has a half width of 3 km, but nothing is injected above about 25 km. We set this upper altitude limit based on the heights of the stratospheric sulfate clouds from explosive volcanic eruptions, which rise buoyantly as do smoke plumes. The Gaussian distribution at the ground (Eq. 3) has a half width of 1 km, assuming that the local boundary layer is relatively shallow. We assume 50% of the soot is contained in each of these distributions (Eq. 2, and Eq.3) for the general case, and for the 1 km impact. For the K-Pg, we assume the soot observed in the distal layer by Wolbach et al (1988, 1990b) was all in the portion of the Gaussian distribution at the tropopause (Eq. 2).

Therefore, the injection profiles are given by:

$$I(g\ s^{-1}km^{-1}) = \frac{I_{T1}}{\eta\sqrt{2\pi}} \left[ e^{\left(-0.5\left(\frac{z-z_{trop}}{\eta}\right)^2\right)} \right] \quad (2)$$

$$I(g\ s^{-1}km^{-1}) = \frac{I_{T2}}{\mu\sqrt{2\pi}} \left[ e^{\left(-0.5\left(\frac{z}{\mu}\right)^2\right)} \right] \quad (3)$$

Here  $I$  is the mass emission rate per km of altitude,  $I_{T1}$  and  $I_{T2}$  are the total mass emitted per second into the upper (Eq. 2) or lower (Eq. 3) altitude range after correcting for the emission altitude range (0-25 km) and grid spacing,  $\mu$  is 1 km,  $\eta$  is 3 km, and  $z_{trop}$  is the altitude of the tropopause.

Geographically, we assume for the K-Pg event that all the surface biomass is set on fire. For the 1 km diameter impact, however, only the region near the impact site would burn as discussed further below.

There is also an issue of how long it takes to inject the smoke. Forest fires often burn for days, advancing along a fire front as winds blow embers far beyond the flames and onto unburned terrain. Mass fires may not spread because powerful converging winds restrict the spread. However, little is known observationally about mass fires, and fires can spread by intense infrared radiation lighting adjacent material. If mass fires are restricted then they will burn only as long as they have fuel. The present above ground global biomass in tropical forests is in the range of 0.6-1.2 g C cm<sup>-2</sup> (Houghton, 2005). The energy content of biomass is on the order of 3x10<sup>4</sup> J/g C or, given the biomass concentration just mentioned, about 3x10<sup>8</sup> J m<sup>-2</sup>. Penner et al. (1986) and Small and Heikes (1988) found that large area mass fires with energy release rates of 0.1 MW m<sup>-2</sup> would have plumes reaching the lower stratosphere. Hence, it would be necessary to assume that the fuel burned in an hour or so to achieve these energy releases. Of course, it might take some time for fires in different places to start fully burning, so considering the entire region of the mass fire, as opposed to a small individual part of the fires, might prolong the energy release considerably. For example, it took several hours for the mass fire in Hiroshima to develop after the explosion of the atom bomb (Toon et al., 2007)

It should be noted that in simulations of stratospheric injections of soot from nuclear conflicts, soot is self-lofted by sunlight heating the smoke (Robock et al., 2007b). However, in the case of the K-Pg impact, if there are other types of particles injected above the soot, which then block sunlight, the soot may not be self-lofted, which will limit its lifetime. The initial soot distribution that is estimated here does not include the effects of self-lofting, which would continue after the initial injection and should be part of the climate simulation.

The final property to specify for soot is the optical constants. This issue is complicated by the possible presence of organic material on the soot (Lack et al., 2012). However, it is known that many of these organics are quickly oxidized by ozone, which is plentiful in the ambient stratosphere. The stratosphere after the impact however, may have become depleted in ozone very quickly, so that the organic coatings might have survived. It is also possible that intense fires, such as mass fires, will consume the organic coatings, which may explain why the production of soot in the fires seems to have been so much more efficient than for normal fires. It may therefore be sufficient to treat the soot as fractal agglomerates of elemental carbon (Bond and Bergstrom, 2006). It is known that the optical properties of the agglomerates will not obey Mie theory. However, one may treat their optical properties as well as their microphysical properties using the fractal optics approach described by Wolf and Toon (2010). The optical constants for elemental carbon may then be used for the monomers. Alternatively, one may add the organic mass to the particles, and treat them using core-shell theory (Toon and Ackerman, 1981; Mikhailov et al., 2006).

Bond and Bergstrom (2006) have thoroughly reviewed the literature on the optical properties of elemental carbon. They conclude that the optical constants are most likely independent of wavelength across the visible, with a value that depends on the bulk density of the particles. Following their range of values for refractive index versus particle density we suggest using a wavelength independent real index of refraction  $n=1.80$  and an imaginary index  $k=0.67$ . We also use these values in the infrared as shown in Figure 3. For the monomers in Tables 1 and 3, we adopt the density suggested by Bond and Bergstrom (2006) for light absorbing material,  $1.8 \text{ g cm}^{-3}$ .

### **2.2.2 Soot from a 1 km impact**

Extrapolations of the soot injection parameters to smaller impactors than the one defining the K-Pg boundary should only involve changes to the mass of soot injected, since the basic properties of the soot at the K-Pg boundary are similar to those of forest fire soot. Therefore, the particle sizes, injection heights, and optical constants recommended in Table 3 for the smaller impact are the same as listed in Table 1 for the Chicxulub impact. The mass of soot injected is estimated from the extrapolations in Toon et al. (1997). For an impactor as small as 1 km diameter, debris from the impact site would not provide sufficient energy to ignite the global biota since the energy of the 1 km impactor is about 1000 times less than that of the Chicxulub impactor. Instead, radiation from the ablation of the incoming object and from the rising fireball at the impact site would ignite material

that is within visible range of the entering object and the fireball. This ignition mechanism is well understood from nuclear weapons tests (Turco et al., 1990). Hence, for a 1 km diameter impactor the fuel load at the site of the impact becomes critical to evaluate the soot release. No soot would be produced from an impact in the ocean, an ice sheet, or a desert. In Table 3 to compute the smoke emitted (28 Tg), we use equation 12 from Toon et al. (1997) to obtain an area of  $4.1 \times 10^4 \text{ km}^2$  for the expected area exposed to high thermal radiation density from the fireball for a 1 km diameter impactor with an assumed energy of  $6.8 \times 10^4 \text{ Mt}$ . We then multiply that area by 3% (the fraction of C in the burned fuel that is converted to smoke) and by  $2.25 \text{ g C cm}^{-2}$ , (the assumed carbon content per unit area of the dry biomass that burns). The user of Table 3 can choose alternate values of the injected soot by scaling linearly to the biomass concentration they chose.

Ivany and Salawitch (1993) suggest that the land average, above ground biomass was about  $1 \times 10^{18} \text{ g}$  (about  $0.7 \text{ g C cm}^{-2}$ ) at the end of the Cretaceous. The current land average, above ground biomass is about  $0.3$  to  $0.44 \text{ g C cm}^{-2}$  (Ciais et al., 2013). An additional  $1$  to  $1.6 \text{ g C cm}^{-2}$  is currently present in the soil, while Ivany and Salawitch suggest  $1 \text{ g C cm}^{-2}$  in the soil in the Cretaceous. Some of the soil biomass may burn in a mass fire. Tropical and boreal forests currently have average biomass concentrations (above ground and in soil) of about  $2.4 \text{ g C cm}^{-2}$ , while temperate forests have about  $1.6 \text{ g C cm}^{-2}$  including soil carbon (Pan et al., 2011). Soil carbon is 30% of carbon in tropical forests and 60% in boreal forests. Together tropical and boreal forests cover 6% of the Earth's surface, and temperate forests 1.5%. These forests cover 26% of Earth's land area. In Table 3 we assume that the biomass that burns is typical of a tropical or boreal forest assuming the soil carbon burns. The reader can make other choices for the biomass by scaling from the fuel load that the reader prefers.

Another modeling issue of concern is the ability of models to follow the initial evolution of the plume. If we assume that half of the 28 Mt of smoke from the 1 km impact is injected over an area of  $4 \times 10^4 \text{ km}^2$ , and over a depth of 6 km near the tropopause (Eq. 2) as  $0.1 \mu\text{m}$  radius smoke particles, the smoke will have an initial optical depth near 4000, and the number density of particles will be about  $10^7 \text{ cm}^{-3}$ . (The other half of the smoke mass injected near the ground (Eq. 3) will likely be removed quickly and have little impact on climate). Intense solar heating at the top of the smoke cloud near the tropopause will loft it, while coagulation will reduce the number of particles by a factor of 2 and increase their size proportionately in only one minute. Hence, one needs to model this evolution on sub-minute time scales to accurately follow the initial evolution. Alternatively, but less accurately, one might spread out the injection in time and space, so that the climate model can track the evolving smoke cloud using typical model time steps.

## 2.3 Nano-particles from vaporized impactors

### 2.3.1 Nano-particles from the vaporized material following the Chicxulub impact

Johnston and Melosh (2012b) find at the end of their simulations of the rising fireball that about 44% of the rock vapor that was created from the K-Pg asteroid impact remained as

vapor rather than condensing to form large spherules. This vapor is about an equal mixture of impactor and asteroid, so the 44% mass fraction is approximately equal to the mass of the impactor. This 44% vapor fraction depends on the pressures reached in the impact, the equation of state of the materials, as well as the detailed evolution of the debris in the fireball. The fate of this vapor phase material is not well understood, and has been little studied. It may simply have condensed on the spherules, or it may have remained as vapor.

Presently, 100  $\mu\text{m}$  and larger sized micro-meteoroids ablate to vapor in the upper atmosphere. Hunten et al. (1980), following earlier suggestions, modeled the condensation of these rock vapors as they form nm-sized particles in the mesosphere and stratosphere. Bardeen et al. (2008) produced modern models of their distribution based on injection calculations from Kalashnikova et al. (2000). Hervig et al. (2009) and Neely et al. (2011) showed that these tiny particles are observed as they deposit about 40 tons of very fine-grained material on Earth's surface per day. It is possible that a similar process occurred after the Chicxulub impact. However, in the Chicxulub case the vaporization occurred during the initial asteroid impact at Chicxulub rather than on reentry of the material after the fireball rose thousands of km into space and dispersed over the globe.

The presence of 15-25 nm diameter, iron-rich material has been recognized in the fireball layer at a variety of sites by Wdowiak et al. (2001), Verma et al. (2002), Bhandari et al. (2002), Ferrow et al. (2011) and Vajda et al. (2015) among others. The nano-phase iron correlates with iridium, is found worldwide, and therefore is likely a product of the impact process. Unfortunately, these authors have not quantified the amount of this material that is present. Berndt et al. (2011) were able to perform very high-resolution chemical analyses, and also report a component of the platinum group elements that arrived later than the bulk of the ejecta, and was probably the result of submicron sized particles. However, they were not able to size the particles, nor quantify their abundance.

In Table 1 we take the upper limit of the injected mass of nano-particles to be  $2 \times 10^{18}$  g. The lower limit is zero. This choice for the upper limit is consistent with the vapor mass left at the end of the simulations by Johnston and Melosh (2012b). We assume an initial diameter of 20 nm, following Wdowiak et al. (2001). We assume the particles are initially injected over the same altitude range as the Type 2 spherules, because we speculate that the small particles would not separate from the bulk of the ejecta in the fireball until the ejecta entered the atmosphere and reached terminal velocity. The mass injected would lead to an optical depth of particles larger than 1000 even if they coagulated into the 1  $\mu\text{m}$  size range. Goldin and Melosh (2009) point out that such an optically thick layer of small particles left behind by the falling large spheres might also be important for determining whether the infrared radiation from the atmosphere heated by the Type 2 spherules is sufficient to start large-scale fires.

The optical properties of the nano-particles are not known. We suggest using the optical properties of the small, vaporized particles currently entering the atmosphere from Hervig et al. (2009). These optical constants are plotted in Figure 3. We also assume that the particles have the density of CM2 asteroids, since Cr isotope ratios suggest that is the composition of the K-Pg impactor (Trinquier et al., 2006). This density is  $2.7 \text{ g cm}^{-3}$ . A significant fraction of the vaporized material may be from the impact site, so using an asteroidal composition to determine the density is an approximation.

666

### 667 **2.3.2 Nano-particles from the vaporized material from a 1 km impact**

668 Johnson and Melosh (2012b) did not comment on the amount of vapor that would be  
669 expected to not condense as spherules from a 1 km diameter impact. From the theory of  
670 impacts, it is expected that an amount of impactor plus target that is about twice the mass  
671 of the impactor would be converted into vapor from a 1 km diameter impact, just as it is  
672 for a 10 km diameter impact. In Table 3 we assume that as an upper limit 35% of the  
673 impactor mass plus an equivalent amount of target material, would be left as vapor after  
674 spherules form. We chose this mass fraction, which is lower than that for the K-Pg object,  
675 because the 1 km impact will have a smaller fireball, and be more confined by the  
676 atmosphere. We also assume the injected particles will have a diameter of 20 nm. From  
677 simple energy balance along a ballistic trajectory we would expect that the vaporized  
678 ejecta in the fireball from a 1 km impact would rise about a thousand km above the  
679 Earth's surface. This altitude is consistent with limited numerical calculations for large  
680 energy releases, which indicate that the vertical velocity of the fireball is not significantly  
681 reduced in passing through the atmosphere (Jones and Kodis, 1982). As the material  
682 reenters the atmosphere, the particles will come to rest when they encounter an  
683 atmospheric mass comparable to their own mass. Hence it is likely that the altitude  
684 distribution of the nano-particles from the 1km impact will be the same as we have  
685 assumed for the K-Pg impactor in Table 1, which is also similar to, but slightly lower in  
686 altitude than the vertical distribution of micrometeorites on present day Earth as  
687 discussed by Bardeen et al. (2008). It is difficult to determine precisely the area that will  
688 be covered by this material as it reenters the atmosphere. If we assume that it takes about  
689 30 min for the debris to reach peak altitude and return to the Earth, and that the plume is  
690 spreading horizontally at about 4 km/s then the debris would enter the atmosphere over  
691 an area of about half that of the Earth. These estimates of area covered are consistent  
692 with the observations of the SL-9 impact collisions with Jupiter, and the plume from the  
693 much less energetic impact at Tunguska, though these are not perfect analogs (Boslough  
694 and Crawford, 1997). The optical depth of the nano-particles from the 1 km diameter  
695 impact averaged over the Earth is estimated for comparison with the estimates of other  
696 types of particles to be relatively large, 1.5, as noted in Table 3.

697

### 698 **2.4 Submicron clastics**

#### 699 **2.4.1 Submicron clastics from the Chicxulub impact**

700 Another clear component of the K-Pg debris layer is pulverized target material. This  
701 clastic material was first recognized from shocked quartz grains (Bohor, 1990), but there  
702 are also shocked carbonate particles from the Yucatan Peninsula in the K-Pg boundary  
703 layer material (Yancy and Guillemette, 2008; Schulte et al., 2008). Because of chemical  
704 alteration of much of this material in the past 65 million years it is difficult to determine  
705 the mass and size distribution directly except for the shocked quartz, which is readily  
706 identified. The shocked quartz grains generally are large and would not have remained  
707 long in the atmosphere. However, the shocked quartz is probably not directly related to  
708 the bulk of the clastics. For instance, within 4000 km of Chicxulub the shocked quartz is  
709 primarily in the few mm thick fireball layer, which is distinct from the several cm or

thicker ejecta layer that is dominated by clastics. The shocked quartz likely came from basement rock, reached higher shock pressures than the bulk of the pulverized ejecta and therefore was distributed globally in the impact fireball along with the melted and vaporized material from the target and impactor. The other pulverized material, in contrast, came mainly from the upper portions of the target along with basement rocks toward the exterior of the crater, and the fragments were distributed locally (within about 4000 km of Chicxulub) in the impact ejecta debris.

The submicron fraction of the clastics is of interest because particles of such size might remain in the atmosphere for months or years and perturb the climate, unlike larger particles that would be removed quickly by sedimentation. For instance, Pueschel et al. (1994) found 3-8 months after the 1991 eruption of Mt. Pinatubo in the Philippines that volcanic dust particles with a mean diameter near  $1.5\ \mu\text{m}$  were optically important in the lower stratosphere in the Arctic.

The optical constants for the injected clastics are suggested from their composition. For the Chicxulub impact the clastic material is largely carbonate evaporates. We suggest using the optical constants of limestone from Orofino et al. (1998). Unfortunately, the values need to be generated from a table of oscillator strengths. They also need to be interpolated into the visible wavelength range. We suggest extending the oscillator predictions into the visible range as done by Querry et al. (1978). The density of limestone is in the range of  $2.1\text{-}2.6\ \text{g cm}^{-3}$ , while dolomite and anhydrite have densities near  $2.9\ \text{g cm}^{-3}$ . Granite has a density near  $2.6\text{-}2.8$ . While each of these materials contribute to the clastic debris, for convenience we assume the pulverized ejecta have a density of  $2.7\ \text{g cm}^{-3}$ .

Pope (2002) and Toon et al. (1997) used two different methods to determine the amount of the submicron-clastic material from the Chicxulub impact. Unfortunately, these estimates disagree by about 4 orders of magnitude, as indicated in Table 5, third row, columns 1 and 2. Toon et al. (1997) used arguments based mainly on impact models, to estimate that more than 10% of the mass of the distal layer ( $> 7 \times 10^{17}\text{g}$ ) is submicron diameter clastics, which would be significant to climate. Pope (2002) estimated that the clastics in the distal layer have a mass that is  $< 10^{14}\text{g}$ . Pope (2002) used data on shocked quartz to constrain the amount of clastics, which in principle is a better approach than using estimates based on a model as in Toon et al. (1997). The amount of clastics of all sizes in the Pope (2002) model ( $10^{16}\text{g}$ ) is only 12-30 times larger than the clastics of all sizes emitted in the relatively small 1980 Mt. St. Helens eruption. Therefore, based on Pope's (2002) analysis, the submicron fraction would not be of significance to climate. Below we attempt to reconcile these two approaches to better determine the amount of submicron clastics.

#### **2.4.1.1 Potential errors in the Toon et al. (1997) estimate of submicron clastics**

Toon et al. (1997) estimated the amount of submicron clastics starting from analytical models of the mass of material injected into the atmosphere by a 45-degree impact. They estimated the mass of melt + vapor per megaton of impact energy ( $\sim 0.2\ \text{Tg/Mt}$ ) and the mass of pulverized material per megaton of impact energy (about  $4.5\ \text{Tg/Mt}$ ). Assuming a  $1.5 \times 10^8\ \text{Mt}$  impact, these formulae suggest a melt + vapor amount of  $3 \times 10^{19}\text{g}$  ( $\sim 1 \times 10^4$

km<sup>3</sup>, assuming a density of 2.7 g cm<sup>-3</sup>) and a pulverized amount of 7x10<sup>20</sup>g (~2.5x10<sup>5</sup> km<sup>3</sup>). While sophisticated impact calculations generally agree with the amount of melt + vapor, not all of it is found to reach high enough velocity to be ejected from the crater. For example, Artemieva and Morgan (2009) investigated a number of impact scenarios that created transient craters with diameters of 90-100 km, which they thought to be consistent with the transient diameter of the Chicxulub crater. Considering those cases with oblique impacts from 30-45 degrees with energies of 1.5-2 x10<sup>8</sup> Mt, they found that the melt was in the range 2.6x10<sup>4</sup> to 3.8x10<sup>4</sup> km<sup>3</sup>. However, the amount that reached high enough speed to be ejected from the crater was in the range 5x10<sup>3</sup> to 6x10<sup>3</sup> km<sup>3</sup> (average 5.6x10<sup>3</sup> km<sup>3</sup>, 1.4x10<sup>19</sup>g, about 2-10 impactor masses). On average, only about twenty percent of the melt and vapor amount escapes from the crater. Therefore, Toon et al. (1997) may have overestimated the amount of melt escaping from the crater by about a factor of 2. It should be noted that in Artemieva and Morgan (2009) the melt exceeds the mass of the distal layer, which is about 4x10<sup>18</sup>g, by about a factor of 5, because much of the melt is deposited as part of the ejecta curtain and never reaches the distal region.

Artemieva and Morgan (2009) find that the total mass ejected from the crater is 1.3x10<sup>4</sup> km<sup>3</sup> (2.9x10<sup>19</sup> g). Assuming that 90% of this material is pulverized rock their results imply that Toon et al. (2007) overestimated the amount of clastic debris ejected from the crater by a factor of about 25. In column 3 of Table 5 we correct the amount of pulverized material to agree with the Artemieva and Morgan (2009) value of 2.9x10<sup>19</sup> g of clastics escaping the crater. It is interesting to note that the clastic mass from Chicxulub is only a factor of about 10 larger than the minimal estimated mass of clastics ejected in the Toba volcanic eruption about 70,000 years ago (Matthews et al., 2012).

Another issue is the fraction of the pulverized debris that is submicron. Toon et al. (1997) computed the amount of pulverized debris whose diameter is smaller than 1 μm from size distributions measured in nuclear debris clouds originating from nuclear tests that were many orders of magnitude lower in energy than the K-Pg impact, and from impact crater studies cited by O'Keefe and Ahrens (1982) based on grain size measurements from craters. Toon et al. (1997) assume that 0.1% of the total clastic material would be submicron. Pope (2002) cited studies of volcanic clouds to conclude that 1% by mass of the pulverized material would be submicron.

Rose and Durant (2009) examined the Total Grain Size Distribution (TGSD) from a number of volcanic eruptions and concluded that the amount of fine ash is related to increasing explosivity of the event. The TGSD is supposed to represent the size distribution as the clastics left the crater. Mt. St. Helens is the most likely of the volcanic eruptions they considered to be relevant to the extreme energy release in a large impact. About 2% of the total ejecta from Mt. St. Helens had a diameter smaller than 1 μm. Since the erupted mass was about 3-8x10<sup>14</sup> g, the submicron mass emitted by Mt. St. Helens was about 6-16x10<sup>12</sup>g. Matthews et al. (2012) considered the Toba eruption, whose clastics are within an order of magnitude of those from Chicxulub. Their data shows that 1-2% of the mass of the clastics is in particles smaller than 1 μm and 2-6% in clastics smaller than 2.5 μm.

In Table 5 we use 2% of the pulverized material as a revised estimate for the fraction of the clastic material that is released as submicron ejecta. This fraction is a factor of 20 larger than the one used in Toon et al. (1997). Hence our revised submicron mass

estimate for the Chicxulub impact (column 3 row 3) is very similar to the one Toon et al. (2007) estimated (column 2 row 3) because, although we lowered the estimate of the clastic mass exiting the crater to agree with Artemieva and Morgan (2009), we increased the estimate of the fraction that is submicron.

A confounding issue is the amount of submicron and other clastics that escapes from the near crater region and is distributed globally. A large fraction of the pulverized debris in the ejecta curtain was removed within 4000 km of the impact crater (Bohor and Glass, 1995), and volcanic ejecta is likewise largely removed near the volcanic caldera. For example, there is 4-8 cm of ash 3000 km from the Toba crater, which is not too different from the thickness of the Chicxulub deposits at a similar distance from the crater. If the removal occurred only by individual particle sedimentation, one could simply take the mass in the smaller ranges of the size distribution and assume it spread to the rest of the globe. However, it is clear from volcanic eruption data that a significant fraction of the submicron debris is removed near the volcano by processes other than direct sedimentation (Durant et al, 2009; Rose and Durant, 2009). These processes include rainout of material from water that condenses in the volcanic plume, and also agglomeration possibly enhanced by electrical charges on the particles. It is likewise clear that such localized removal occurred after the K-Pg impact. Yancy and Guillemette (2008) describe accretionary particles that make up a large fraction of the debris layer as far as 2500 km from the Chicxulub crater. These agglomerated particles, which range in size from tens to hundreds of  $\mu\text{m}$ , are composed mainly of particles with a radius of 1-4  $\mu\text{m}$ . While largely composed of carbonate, the particles are enriched in sulfur.

One can use the size distributions from volcanic data, along with the total clastic mass ejected from Chicxulub to compute the particle agglomeration, and thereby follow the particles as they spread across the Earth. Such work is now being done for volcanic events, for example by Folch et al. (2010). They find that they can successfully reproduce mass deposited on the surface from the Mt. St. Helens eruption by including agglomeration. However, such calculations for Chicxulub are difficult for several reasons: the large clastic masses involved exceed the mass of the atmosphere for a considerable distance from the crater, so the debris flows cannot be reproduced in standard climate models; the complexity of the distribution of material in the plume with some material reaching escape velocity and other parts being hurled over a substantial fraction of the planet make it difficult to determine the spatial distribution of the material, and some material is likely lofted well above the tops of most climate models; and the presence of clastics, melt and rock vapor together with sulfur and water produces a chemically complex plume.

Eventually it will be necessary to use detailed non-hydrostatic, multiphase plume models including agglomeration to better understand the distribution of Chicxulub ejecta. In the meantime for climate modeling we suggest placing the clastic mass in Table 5 ( $2.9 \times 10^{19}$  g) in a circular area with radius of 4000 km, which is 22.4% of the area of Earth. This will result in a column density of  $25 \text{ g cm}^{-2}$ , or a layer thickness of about 10 cm. The mass density of the atmosphere is about  $1000 \text{ g cm}^{-2}$ , so this is about a 2.5% perturbation to the mass of the atmosphere. In reality the mass is concentrated near the crater as shown by Hildebrand (1993). However, the observed mass density is relatively constant between 1000 and 4000 km. The initial vertical distribution of this material may be very

complex due to density flows within several hundred km of the crater. We suggest initializing models assuming an injection with an altitude independent mass mixing ratio of about 2.5%. Given our suggested vertical distribution 90% of the material will initially lie in the troposphere. Tropospheric material is unlikely to become globally distributed even if it escapes agglomeration, because it will quickly be removed by rainfall.

As an alternative to the complexity of modeling the loss of this material in the troposphere and considering the entire size distribution, we suggest simply placing an appropriate mass into the stratosphere. The values for a stratospheric injection are given in the bottom row of Table 5 and the first row of Table 1. For illustration, we have estimated the final optical depth assuming that 10% of the submicron material (the amount placed into the stratosphere) will escape removal. For a size distribution we suggest using the smaller size mode measured in the stratosphere after the Mt. St. Helens eruption as summarized by Turco et al. (1983). This size distribution is log-normal (Eq. 1), with a mode radius of  $0.5 \mu\text{m}$  and a standard deviation of 1.65. The estimated optical depth of 88 is very large, even though the submicron clastic material in this estimate is only about 1% of the mass of the distal layer.

#### **2.4.1.2 Potential errors in the Pope (2002) estimate of submicron clastics**

Pope (2002) determined the amount of clastics by modeling the amount of quartz in the distal layer. He found that he needed an initial injection of about  $5 \times 10^{15}$  g of quartz to match the distribution of quartz mass with distance from the impact site. It is not clear how good this estimate is because the removal rate of material in large volcanic clouds, a possible impact analog, does not occur by individual particle sedimentation, but rather by settling of agglomerates (Folch et al., 2010). Hence removal in the region near the impact site may have been larger than Pope estimated, requiring a larger volume of quartz; or the removal of clastics may be different than that of quartz. The value in Artemieva and Morgan (2009) for the pulverized material ejected from the crater is 3 orders of magnitude larger than the estimate of Pope (2002). Most of this material is in the ejecta curtain, not in the impact fireball, and so is deposited close the impact crater. The shocked quartz is primarily associated with the impact fireball, so the bulk of the pulverized material may not be seen in Pope's analysis.

Pope assumed that quartz composed 50% of all the clastic debris, so that all of the clastics injected weighed about  $10^{16}$  g. This number is about two orders of magnitude less than the clastics from the Toba eruption (Matthews et al., 2012), and more than 3 orders of magnitude less than the Artemieva and Morgan (2009) estimate for clastics from the Chicxulub impact.

The assumption by Pope (2002) that quartz is 50% of all the clastics is likely in error. There is no reason to think there is much quartz in the upper layers of sediment at the Chicxulub site. In the stratigraphic columns shown by Ward et al. (1995) the pre-impact sediments at Chicxulub consist of approximately 3 km of Mesozoic carbonates and evaporites with ~3-4% shale and sandstone. Therefore, it is more likely the quartz originates from the basement rocks. There is also not a strong connection between the physical processes that distributed the quartz (the impact fireball, with high ejection

velocity), and those that distributed the pulverized material (the ejecta curtain with low velocity).

It is possible that the quartz to clastics ratio is determined by the ratio of quartz to total debris in the samples closest to Chicxulub, since these may have suffered the least removal by sedimentation. Pope suggests these intermediate distance layers contain about 1% quartz, but only considers the fireball layer, which is less than 10% of the total ejecta layer within 1000 km of the crater. The remainder of the intermediate distance layer contains little quartz, so the clastics could be more than 1000 times the mass of the quartz. It is not clear that 1000 is an upper limit to the ratio of clastics to quartz because the quartz and pulverized material move along different paths in the debris cloud. If we accept this ratio of 1000 for the ratio of clastics to quartz, the mass of clastics from Pope's analysis would be  $5 \times 10^{18}$  g, which is within a factor of 6 of the Artemieva and Morgan (2009) value. If 1% of this mass is submicron then  $5 \times 10^{16}$  g of submicron clastics would have been injected into the upper atmosphere.

#### **2.4.1.3 Reconciliation of Pope (2002) and Toon et al. (1997) estimates of submicron clastics**

Table 5 shows that the new estimate of submicron mass following the procedure of Toon et al. (1997) agrees with the new estimate following the procedure of Pope (2002) within 20%. The new estimate is about 12 times less than the Toon et al. (1997) value mainly because Toon et al. (1997) did not consider that most of the pulverized mass would not be ejected from the crater. The new application of the Pope (2002) approach leads to estimated submicron dust emissions that are about 500 times larger than the one originally derived by Pope (2002). The major difference is that we have assumed the ratio of quartz to clastics is about 1000, rather than 1 as assumed by Pope (2002). Despite the perhaps coincidental agreement of these two estimates, there is substantial uncertainty in the true mass of submicron clastic particles in the K-Pg distal layer. Observations of the submicron material in the distal layer are needed.

#### **2.4.2 Submicron pulverized rock from a 1 km diameter impactor**

In order to determine the properties of the pulverized ejecta from a 1 km impactor, we use the pulverized mass injection per Tg of impact energy from Toon et al. (1997), but reduce it by the factor of 25 discussed earlier to account for the fraction of the clastic mass with enough velocity to escape the crater. This procedure yields a clastic mass of  $1.3 \times 10^{16}$  g. For reference, the volume of clastics from the eruption of Mt. Tambora in 1815 is estimated to have been about  $150 \text{ km}^3$ , which is a mass of about  $3 \times 10^{17}$  g. Hence the Tambora eruption likely surpasses the clastics from the hypothetical 1 km diameter impactor by more than a factor of 10. The same size distribution for the clastics is recommended for the 1 km impact and the Chicxulub impact, since it seems to hold for a range of volcanic events from Mt. St. Helens to Toba, which span the 1 km diameter impactor in terms of clastics. We also suggest that the mass be initially mixed uniformly in the vertical above the tropopause. According to Stothers (1984) the Tambora clastics were deposited in layers that are centimeters in thickness at distances 500 km from the volcano. Accounting for the drift of the ash downwind, the area of significant ash fall was about  $4.5 \times 10^5 \text{ km}^2$ . If this same area is used for the initial injection of the clastics for

the 1 km impact, then the column mass concentration is about  $8.7 \text{ g cm}^{-2}$ , which in turn is slightly less than 1% of the atmospheric column mass. The estimated optical depth of the clastics in Table 3 is about 25% of the optical depth from nano-particles originating from vaporized rock. Given that these materials are much less absorbing than soot, and lower in optical depth than nano-particles they can probably be neglected in estimates of the climate changes due to a 1 km diameter impact on land.

### **3. Gas injections**

There are a large number of gases that might be injected into the atmosphere after an impact and might be important to atmospheric chemistry, climate, or both. These can originate from the impactor itself, from ocean or ground water, or from the target sediments. They may also originate in response to environmental perturbations, such as wildfires, or atmospheric heating from the impact fireball and ejecta. Various estimates have been made for each of these sources. However, clear evidence from the distal layer is not available for any gases of potential interest. Some gases, such as carbon dioxide, would have stayed in the gas phase rather than condensing into particulate form. Other gases, such as those containing sulfur, may have reacted on the particles composing the distal layer, or formed independent particles. In either case sulfur is so common in the environment it is difficult to detect an injection. For these reasons all the gas phase injections are uncertain. Below, we first discuss the chemical content of each of the potential sources of gases, and then we discuss the likely amounts of each material injected following an impact. Relevant ambient abundances are given in Tables 2 and 4 along with estimated injections for the Chicxulub impact and a 1 km impact. The ambient masses are given to assist the reader in understanding the magnitudes of the injections. Generally ambient concentrations are given in the literature in terms of the mixing ratio. To compute the masses we assume the ambient mixing ratios are constant over the whole atmosphere, or the stratosphere. We then convert the volume mixing ratio to the mass mixing ratio using the molecular weight and then multiply by the mass of the atmosphere above either the surface, or tropopause to obtain the total mass of the gas. The ambient abundances assume the current stratospheric mixing ratio of Cl is 3.7 ppbv (Nassar et al., 2006), Br is 21.5 pptv (Dorf et al., 2006), inorganic I is 0.1pptv (upper limit from Bosch et al. 2003),  $\text{CO}_2$  is about 395 ppmv, and methane is about 1.8 ppbv. Stratospheric S, taken from the Pinatubo volcanic eruption, is about 10 Tg (Guo et al., 2004), reactive nitrogen,  $\text{NO}_x$ , in the stratosphere is difficult to quantify simply. Instead we compare with the ambient abundance of  $\text{N}_2\text{O}$  in the stratosphere, about  $2 \times 10^{14} \text{ g N}$ .  $\text{N}_2\text{O}$  is a major source of  $\text{NO}_x$ .

### **3.1 Impactor**

#### **3.1.1 Composition of the impactor**

Kring et al. (1996) summarized the S, C, and water contents of a large number of types of asteroids. Trinquier et al. (2006) found from chromium isotopes that the Chicxulub impactor was most likely a carbonaceous chondrite of CM2 type. Such asteroids have 3.1wt % S, 1.98 wt% C, 11.9 wt% water, and a density of  $2.71 \text{ g cm}^{-3}$ . Over the range of chondrites, which constitute 85% of meteorite falls, S varies from 1.57 to 5.67 wt%, C from 0.04 to 3.2 wt %, and water from 0.2 to 16.9 wt %. Kallemeyn and Watson (1981)

report that by mass CM carbonaceous chondrites contain about 4ppm Br. Goles et al (1967) report that Cl ranges from 190-840 ppm of carbonaceous chondrites, Br ranges from 0.25 to 5.1 ppm, and Iodine ranges from 170 to 480 ppbm. Table 6 summarizes the composition of asteroids using values for CM2 type carbonaceous chondrites from Kring et al. (1996) for S, C, and water, and for the Mighei (the CM2 type example) from Goles et al. (1967) for Cl, Br and I.

### **3.1.2 Gases from the impactor**

Tables 2 and 4 indicate the direct contributions from 1 and 10 km impactors of a number of chemicals, as discussed further below. We assume that the entire 10 km or 1 km diameter impactor melted or vaporized so that all of the gases are released. For the 10 km impactor these gases would have been distributed globally in the hot plume along with the melt spherules within hours. They would reenter with the same vertical distribution as the Type 2 spherules. For the 1 km diameter impactor, the initial injection may have only covered half the Earth, with global distribution over days via wind, after reentry into the upper atmosphere.

We further assume that the vapors under consideration do not react with the hot mineral grains either in the plume or in the hot layer at the reentry site. In fact, given the large particle surface areas in the atmosphere over the globe it is possible that there was a significant transfer of material from the gas phase to the surfaces of the mineral grains in a short period of time.

As pointed out by Kring et al. (1996) and Toon et al. (1997) the S in a 10 km diameter impactor would exceed that from the Mt. Pinatubo volcanic injection by a factor above 1000. Even a 1 km diameter carbonaceous chondrite could deliver several times as much sulfur to the atmosphere as did the Mt. Pinatubo eruption in 1991. Stratospheric water could be enhanced by a factor of more than 100 from the water in a 10 km impactor. Cl could be enhanced by factors above 500, Br by almost 500, and I by more than 50,000. However, there is not enough C in a 10 km asteroid to affect the global carbon cycle significantly.

Many investigators have pointed to sulfate as an important aerosol following the Chicxulub impact. Tables 1 and 3 compare the mass of sulfur from the impactor with the mass of the spherules and nano-particles. The optical depth, which controls the climate change following the impact, and the particle surface area, which likely controls chemistry, are approximately linear with the mass. In our estimates, the sulfate coming directly from the asteroid could have a large optical depth assuming it was not removed on the spherules, or large clastics.

## **3.2 Seawater**

### **3.2.1 Composition and depth of seawater**

The composition of seawater is given in Table 6 (Millero et al., 2008). It is thought that injections of water into the upper atmosphere will lead to droplet evaporation, with small crystals of salt left behind. If liquid water is left after a massive injection of water, the droplets will likely freeze leaving salt behind as particles embedded in ice crystals.

Vaporization of water during the impact may leave behind salt crystals, or the salts may decompose into their components. As discussed by Birks et al. (2007), complex simulations are needed to determine how much material is freed from the salt particles to enter the gas phase where it might destroy ozone. In Tables 2 and 4 we list the total amounts of several interesting chemicals that might be inserted into the stratosphere. However, all of them except water vapor are likely to be in the form of a particulate until photochemical reactions liberate them.

A significant uncertainty related to any oceanic contribution to atmospheric composition is the depth of the ocean in relation to the size of the impactor, and the water content of sediments at the crater site. The depth of the ocean at Chicxulub at the time of the impact is not known. Many investigators have referred to it as a shallow sea. However, Gulick et al. (2008) estimates that the water depth averaged over the impact site was 650 m, which is considerably deeper than earlier estimates. We use a water depth of 650 m in Table 2 to estimate the amounts of material injected by Chicxulub. A 1 km diameter impactor is smaller than the average depth of the world oceans, which is about 3.7 km.

### **3.2.2 Gases from Seawater-Chicxulub**

For the Chicxulub impact, Pope (1997) assumed that the 650 m depth of seawater within the diameter of the impactor (10 km) will be vaporized, follow the path of the Type 2 spherules, and reenter the atmosphere globally. In Table 2 we compute the water vaporized following the equations in Toon et al. (1997). These equations, assuming an impact velocity of  $20 \text{ km s}^{-1}$ , led to an order of magnitude greater injection of water than using Pope's estimate. The vaporized water is 0.4 times the impactor mass. During the vaporization of the seawater we assume the water will be present as water vapor, and that the materials in the water will be released as vapors. Some of these materials likely would react quickly with the hot minerals in the fireball or later with the hot minerals in the reentry layer.

It is also likely that a considerable amount of water was splashed into the upper atmosphere. Ahrens and O'Keefe (1983) estimated that the water splashed above the tropopause from a 10 km diameter impact into a 5 km deep ocean would be 30 times the mass of the impactor. We assume that the amount of water splashed above the tropopause will scale linearly with the depth of the ocean. Therefore, about 4 times the impactor mass of water may have been splashed into the upper atmosphere. Much of this water may immediately condense and rainout, as discussed in Toon et al. (1997). However, some of the dissolved salts may be released if some of the water evaporates. The assumed injection of gases, and particulates that might become gases, from the ocean is summarized in Table 2 for the Chicxulub impact.

### **3.2.3 Gases from Seawater-1 km asteroid**

No seawater is injected by the 1 km diameter asteroid impact on land. If a comet hit the land there would be a water injection.

Pierazzo et al. (2010) estimated that 43 Tg of water would be injected above 15 km by a 1 km asteroid impact into the deep ocean. Of this water, 25% is in the form of vapor and 75% in the form of liquid water. In their modeling the water was assumed to be distributed with a uniform mixing ratio from the tropopause to the model top. It was also

spread uniformly over an area 6200x6200 km in latitude and longitude. Using the equations in Toon et al. (1997) for the vaporized water produces a value which is 60% of the vaporized water from the detailed modeling used in Pierazzo et al. (2010). Given these water injections we use the composition of sea water to determine the injections of the various species. Pierazzo et al. (2010) estimate injections of Cl and Br that are more than an order of magnitude smaller than ours because they consider the amounts that have been converted into gas phase Cl and Br by photochemical reactions in the atmosphere, while we estimate the total injections, which initially are likely to be in the particulate phase.

### **3.3 Impact Site**

#### **3.3.1 Composition of the impact site**

The sea floor at the Chicxulub impact site, like the modern Yucatan, contained abundant carbonate and sulfate rich deposits. Ward et al. (1995) conclude that 2.5-3 km of sedimentary rock were present at Chicxulub, composed of 35-40% dolomite, 25-30% limestone, 25-30% anhydrite, and 3-4% sandstone and shale. The dolomite and limestone are no doubt porous. Pope et al. (1997) estimate the carbonates in the Yucatan have a porosity of 20%. The pores would have been filled by seawater since the sediments were submerged. This ground water produces an equivalent water depth of about 400 m. The carbon content of limestone is 12% by weight, and of dolomite 15% by weight. The sulfur content of anhydrite is 23.5% by weight. To our knowledge, trace species such as Br, Cl, and I have not been reported for these sedimentary rocks, but would be present in the seawater in the pores.

#### **3.3.2 Gases from the impact site**

For the 10 km Chicxulub impact we follow Pope et al. (1997) for the abundances of S and C assuming 30% anhydrite, 30% limestone and 40% dolomite. The composition of the impact site is given in Table 6. We ignored species other than S and C that might be in the target material. It is difficult to follow the target debris since some of it is vaporized, and some melted. We follow Pope (1997) and assume that the upper 3 km of the target is vaporized within the diameter of the impactor. The gases within this volume of vaporized material are assumed to be released, and to follow the trajectories of the Type 2 spherules. Pope et al. (1997) estimated the amount of material that would be degassed from target material that was melted or crushed in a large impact. We use the values from Table 3 of Pope et al. (1997) for out of footprint vapors, in our Table 2 for the degassed impact site emissions. We also assume that the granite underlying the impact site does not contribute.

The source gases from a 1 km land impact would depend on the composition of the impact site, so we do not list values in Table 4. We assume nothing would be liberated from the sea floor in a 1 km impact in the deep ocean.

### **3.4 Fires**

#### **3.4.1 Composition of Smoke**

It is well known that forest fires emit a wide variety of vapors into the atmosphere. Andreae and Merlet (2001) provide emission ratios (g of material emitted per g of dry biomass burned) for many vapors expected to be important in the atmosphere as listed in Table 6. As discussed in section 2.2.1, the soot emission may have been enhanced relative to wildfire estimates by Andreae and Merlet (2001) after the Chicxulub impact because the impact-generated fires were mass fires. We do not consider any enhancements of the gas phase emission ratios, but they may also be impacted by fire intensity or the types of plants making up the biomass.

### **3.4.2 Gases from Fires**

In Tables 2 and 4 we computed the burned mass from Chicxulub assuming that  $1.5 \text{ g cm}^{-2}$  of dry biomass burns over the entire land surface area of the Earth, and then used the emission factors from Andreae and Merlet (2001) to obtain the gas phase emissions. For a 1 km impact we assume the area burned is  $4.1 \times 10^4 \text{ km}^2$  (Toon et al., 1997), and the dry biomass is  $2.25 \text{ g C cm}^{-2}$ . We then used the emission ratios from Andreae and Merlet (2001) to compute the gas phase emissions. Comparing the gas phase emissions from fires in Tables 2 and 4 with ambient values indicates that there would be large perturbations for all gases for the 10 km diameter impact. Only iodine is significantly perturbed for the 1 km impact. For the gas phase emissions we suggest using the same vertical profile as suggested for soot earlier. The emissions would only occur over the region near the impact site for the 1 km impact.

### **3.5 Gases generated by atmospheric heating**

The energy deposited in the upper atmosphere by the initial entry of the bolide, as well as by the rising fireball, may have converted some  $\text{N}_2$  to  $\text{NO}_x$ . Early studies suggested that a large fraction of the impact energy would be put into the lower atmosphere, which in turn led to suggestions that a large amount of nitrogen oxides would be produced from the heated air. However, it is now understood that most of the energy release from an impact to the atmosphere will occur at high altitude from reentry of spherules and other debris. Toon et al. (1997) reviewed the various ways in which  $\text{NO}_x$  might be generated following an impact, largely following Zahnle (1990). They concluded that  $3 \times 10^{16} \text{ g}$  of NO might be produced from the atmosphere for a 10 km diameter impact with about half coming from the plume at the impact site, and half from the reentry of material across the Earth. We have recorded this value in Table 2. For comparison, Parkos et al. (2015) conducted detailed evaluations of the  $\text{NO}_x$  produced by the infalling spherules and concluded the spherules could produce  $1.5 \times 10^{14}$  moles of  $\text{NO}_x$  ( $3 \times 10^{15} \text{ g}$  if the  $\text{NO}_x$  is in the form of NO) which they further concluded was not sufficient to acidify ocean surface waters. In Table 2 we use the Toon et al. (1997) injection of NO since it includes both source mechanisms. According to Zahnle et al. (1990) a 1 km impact on land might produce  $0.6 \times 10^{14} \text{ g}$  of NO, largely in the hot plume at the impact site. This value is entered in Table 4. For comparison, we note that Pierazzo et al. (2010) suggested that the mass of NO produced by a 1 km ocean impact is about  $0.39 \times 10^{14} \text{ g}$ .

### **3.6 Discussion of gas injections**

Some of the gas phase sources just discussed are easy to apply to an impact. For example, the emissions from fires simply depend on the area burned, the fuel loading and the emission factors.

Other sources of gases are more difficult to evaluate. Since we have no measurements for large impacts, the form of emission can be uncertain. For example, sulfur could be injected as  $\text{SO}_2$  or  $\text{SO}_3$ . Another difficulty that comes in understanding the contribution of target material to gases, such as  $\text{SO}_2$ , is the pressure needed to vaporize the material. Pope (1997), for example, adopted pressures above 70 GPa to vaporize carbonate, 100 GPa for complete vaporization of anhydrite, and 10 GPa for water vaporization from pores. These vaporization pressures are higher than suggested by early researchers, leading to lower amounts of target vaporized. Pierazzo et al. (2003) redid the impact calculations and also estimated the amounts of materials that might be released, which are close to those estimated by Pope et al. (1997). The altitude distribution of the ejecta varies with the source of the material. Finally the chemical form of the emission varies with thermochemistry in the ejecta plume or fireball, and interactions with hot mineral surfaces, and for some materials exposure to high temperature on reentry.

Tables 2 and 4 summarize our choices for the injections of the various gases. For each type of source we also specify the altitude of the expected injection, using a reference to Tables 1 and 2 for the particle injections. We assume all of the impactor mass entered the rising fireball, so it would be injected near 60 km altitude along with the spherules. In some cases, for example for the degassed target material and for splashed seawater, we consider the material to have been uniformly mixed above the tropopause. For materials coming from fires we assume the same vertical injection as for soot.

As has been pointed out many times (Kring, 1996; Toon et al., 1997; Pope et al., 1997; Pierazzo et al., 2003) the sulfur injection from a 10 km impactor might be thousands of times greater than that from the Pinatubo eruption, and also was likely larger than the injection from the massive Toba eruption by a factor between 10 and 100. Our sulfur injection from the target material is about half that of Pope's (1997) estimate of  $10^{17}$  g and slightly less than Pierazzo et al's (2003) estimate for a 15 km diameter impactor of  $7.6 \times 10^{16}$  g. Our sulfur injection from the asteroid itself is within the range suggested by Pope et al. (1997) of  $2.7\text{--}5.9 \times 10^{16}$  g. Interestingly, the sulfur injection we estimate for Chicxulub is about 10 times greater than the yearly emission estimated by Schmidt et al. (2016) for a large flood basalt from the Deccan traps. Of course, the flood basalt might continue for a decade or more, bringing the total sulfur emission close to that from the Chicxulub impact. Table 4 suggests that the sulfur injection from a 1 km impact would be several times greater than that from the Pinatubo eruption, but that would be only a modest injection relative to historical volcanic eruptions. In Table 1 and Table 3 we assume the injected sulfur gas is converted into sulfate. If so it would yield a large optical depth for the Chicxulub impact. However, for both the 1 km and Chicxulub impacts, the sulfur injection, if converted to sulfate, would be an order or magnitude less massive than the nano-particles. Therefore, the sulfate would be an order of magnitude less important optically than the nano-particles. While it might exceed the soot mass slightly, soot is much more important optically than sulfate, which is transparent at visible wavelengths. Therefore, the sulfate in our model is of relatively little importance optically, unless the sulfur remains in the air after the other particles are removed.

Our estimated C injection (in the form of CO<sub>2</sub>) is dominated by emissions from forest fires. We have the same emission from the impactor as Pope (1997), but we have less than half the emission from the target material as Pope (1997) or Pierazzo et al. (2003). All these studies suggest a small impact perturbation relative to the CO<sub>2</sub> 65 million years ago, which was several times larger than now.

The water vapor injections in Tables 2 and 4 are very large compared with ambient values in the stratosphere. However, most of the water is from fires, and half will be injected into the troposphere where it will be quickly removed. The water from the impactor and target is modest, about 1 cm as a global average depth of rain. The typical rainfall averaged over the current Earth is about 3 mm day<sup>-1</sup>. The emissions from the impactor and from vaporized seawater, both of which would have been injected globally at the same altitudes as the Type 2 spherules, are capable of saturating the entire ambient stratosphere. Our water injection is similar to that estimated by Pope (1997), and Pierazzo et al. (2003). While the water vapor has been largely ignored in previous work on the Chicxulub impact, it has the ability to alter the thermal balance of the stratosphere by emitting and absorbing infrared light. Water vapor may have been a factor in the radiation of thermal energy to the surface during the first few hours after the K-Pg impact, since Goldin and Melosh (2009) sought an infrared absorber to prevent radiation from escaping from the top of the atmosphere. Some of the particles in the stratosphere might be removed by precipitation, but the mass of water injected is comparable to the mass of the nano-particles and spherules. Therefore, removal by precipitation is probably not significant since if the water condenses on all the particles it will add only a small mass, and increase the fall rate only slightly, while if water condenses on only a subset of the particles it will remove only a subset. The water injection by the 1 km diameter impact on land is about 15% of the ambient water, but might still lead to some significant perturbations if it is injected into the upper stratosphere. The 1 km impact in the deep ocean could inject about 40 times the ambient water into the stratosphere (Pierazzo et al., 2010), and water should be considered in simulations of such impacts.

For the 10 km diameter impactor, there are injections of Cl, Br, and I that exceed the ambient values by orders of magnitude. There are significant sources for all three halogens from fires, the impactor and seawater, so it seems inescapable that large injections would have occurred. The injections of NO<sub>x</sub> from fires, and from heating the atmosphere are also very large compared with ambient values. For instance, Table 2 shows the NO<sub>x</sub> injections are one to two orders of magnitude larger than the stratospheric burden of N<sub>2</sub>O, the principle source of NO<sub>x</sub>. For the 1 km diameter land impact only the injections of I and NO<sub>x</sub> appear large enough to perturb the chemistry of the stratosphere. However, as discussed by Pierazzo et al. (2010) significant Cl and Br injections could occur for a 1 km impact in the ocean. Seawater injections of Cl, Br, I, and S are complicated because the salts may be injected in particulate form.

#### **4. Implications for climate, atmospheric chemistry and numerical modeling, and suggestions for future data analysis**

Since the discovery of the K-Pg impact by Alvarez et al. (1980), many papers have speculated on which of the many possible effects of the impact on the environment could

have caused the mass extinction. It has become fashionable to claim that one or another effect is dominant. However, it is quite likely that several effects overlapped, each of which might have been devastating to a particular species or ecosystem, but which together made survival very difficult for a broad range of species distributed over the globe. Here we summarize the environmental perturbations we find likely. However, there are many uncertainties, and additional data are needed. We outline the data that would be useful to obtain from the geologic record, and summarize it in Table 7. Also, models have barely scratched the surface of what is possible in better understanding of the post impact environment. We summarize the types of modeling work that would be interesting to pursue. We extend these ideas to smaller impacts since more than 50 impacts of kilometer-sized objects may have occurred since the extinction of the dinosaurs.

Table 1, shows that spherules, soot, nano-particles, submicron clastics, and sulfates each may have had very large optical depths. An optical depth greater than unity could have serious consequences for the environment if maintained for very long. Each of these materials was likely present in the atmosphere, so they may have interacted.

The spherules are unlikely to have changed climate directly because they would have been removed quickly from the atmosphere by sedimentation due to their large size. However, these particles, together with the other impact debris with significant mass, likely heated the upper atmosphere to temperatures between 1000 and 2000K. The high temperature upper atmosphere would then have irradiated the surface with near infrared radiation, causing forest fires. Wolbach et al. (1985) first recognized that the global biota likely burned after the impact, and Melosh et al. (1990) identified the mechanism for starting the fires. The recent work by Goldin and Melosh (2009) identified some complexities in the ignition mechanisms that need further work to be understood. They pointed out that the light might be blocked by the large spherules falling below the heated atmospheric layer. However, this is a complex problem since water vapor, and vaporized impactor would have been present to block radiation escaping to space. Also convection should occur in such a strongly heated layer, which would act to retard the fall of the particles as it does for hailstones in tropospheric convection. Moreover, the mass of debris injected at 70 km, as assumed by Goldin and Melosh (2009), greatly exceeds the mass of air. This mass distribution is unstable and would lead to rapid stirring of the atmosphere down to 50 km. These issues all deserve further study with suitable models. Furthermore, evidence for the nano-particles should be sought as discussed further below.

Robertson et al. (2004) argued that large dinosaurs and other unsheltered animals could have been killed immediately by the radiation from the sky and the subsequent fires. However, it is possible there were refugia on the land, either in regions where spherules did not reenter the atmosphere, as suggested by Kring and Durda (2002) as well as Morgan et al. (2013), or in regions that happened to have heavy cloud cover which may have blocked the radiation. To better understand the possibility of refugia, more complete evidence for the global distribution of spherules would help resolve their possible non-uniform deposition, as suggested in Table 7. It is known that iridium was perturbed worldwide following the K-Pg impact. Although iridium concentrations are spatially variable for a number of reasons, they are basically homogenous over the Earth and do not fall off with distance from the impact site, or at high latitudes. Similar data on

spherules would be useful to determine if the spherules were injected everywhere, or in special places. Numerical values of the spherule concentrations and size distributions to augment the values noted by Smit (1999) would also be of value, as noted in Table 7. Models of the transmission of the light from the hot debris layer above 60 km through dense water clouds and the response of the clouds to the heating would be also useful. It has long been recognized that intense thermal radiation and fires could not have been the only extinction mechanisms at work, since the mass extinctions in the oceans could not have occurred in this way, but instead were likely due to the low light levels preventing photosynthesis (Milne and McKay, 1982; Toon et al., 1982; Pollack et al., 1983; Toon et al., 1997; Robertson et al., 2013b). The low light levels would have been caused by the high optical depths of the soot and nano-particles that remained suspended in the air for a year or more after the impact.

We know from the work of Wolbach et al. (1985; 1988; 1990a; 1990b; 2003) that there is abundant soot in the K-Pg distal layer. It is highly likely that the soot originated from wildfires (Robertson et al., 2013a), but its origin is of secondary concern for climate. The widespread distribution of the soot in the layer, and the small size of the particles indicate this material was almost certainly global in extent. Wolbach et al. (1988; 1990b) show that soot and iridium are tightly correlated across the K-Pg distal layer. The soot and iridium in the distal layer must have been deposited within a few years of the impact, since small particles will not stay in the air much longer. Therefore, any fires must have been within a year or two of the impact. As noted in Table 7, further examination of the distributions of soot, iridium and spherules might clarify how long these materials remained in the atmosphere, which is expected to be days for the spherules, and a few years for the soot and iridium on small particles. Once in the water column, spherules would fall to the bottom in days or weeks. However, in the absence of fecal pellets formed by plankton around the soot, it would take decades for soot to reach the ocean depths by falling. Currents would likely carry the soot down rather than gravity.

The amount of soot in the K-Pg distal layer would produce a very high optical depth when it was in the atmosphere. The transmission of light depends not only on the optical depth, but also on the single scattering albedo of the particles. The single scattering albedo measures the fraction of the light that is scattered, or absorbed. Scattering light, which occurs from sulfates that absorb sunlight only weakly, is not nearly as effective in changing climate as absorbing light.

As discussed by Toon et al. (1997), soot with an optical depth of 100 would prevent any sunlight from reaching the surface—it would be pitch black. No climate simulations of such large soot optical depths have ever been conducted. However, there have been simulations for optical depths in the range of 0.05-1, which show temperatures dropping to ice age conditions within days, precipitation falling to 50% of normal, and the ozone layer being destroyed as discussed further below (Robock et al., 2007a,b; Mills et al., 2008, 2014). There are a number of complexities inherent in climate calculations for soot. For example, it is important to know how long the soot remained in the atmosphere in order to determine how long photosynthesis may have been retarded in the oceans. The lifetime of the soot in turn may depend on the size of the soot particles, their shape, the amount of rainfall in the lower atmosphere, and the amount of sunlight reaching the soot. The amount of sunlight reaching the soot matters because heating the soot also heats the

surrounding air, causing it to rise and loft the soot to high altitudes, where it is protected from rainout (Malone et al. 1985; Robock et al. 2007a,b). These issues can be considered in modern climate models.

Much of the vaporized impactor and target material is thought to have re-condensed to 250  $\mu\text{m}$ -sized spherules (O'Keefe and Ahrens, 1982; Johnson and Melosh, 2012b), which are observed, but a significant fraction may have remained as nanometer sized grains (Johnson and Melosh, 2012b). Iron-rich, nano-phase material with a diameter of 15-25 nm has been identified in the fireball layer at a variety of sites by Wdowiak et al. (2001), Verma et al., (2002), Bhandari et al. (2002), Ferrow et al. (2011) and Vajda et al. (2015) among others. However, the abundance of this nano-phase material is not yet constrained by observations. As noted in Table 7, it is important to quantify the abundance of this nano-phase material, and to confirm that it is the remnant of the vaporized target and impactor. If the amount of vapor remaining at the end of the Johnson and Melosh (2012b) calculation is roughly the amount that remained as rock vapor in the atmosphere, given the optical depth estimate in Table 1 and its input location in the upper atmosphere above the soot generated by forest fires, this nano-phase material would be the dominant source of opacity for changing the climate, and would also greatly affect the amount of radiation emitted to the surface that could start wildfires in the hours following the impact. The material contains iron, so it is likely to have been a good absorber of sunlight. Alternatively, this material might have attached itself to the large spheres and been quickly removed, though this seems unlikely since the large spheres would separate gravitationally from the smaller material within hours. No one has yet considered the effect of this nano-phase material, which is distinct from the clastics envisioned by Toon et al. (1997) and Pope (2002), on the environment after the K-Pg impact.

The most massive part of the ejecta from the K-Pg crater consisted of clastics: crushed and pulverized material. Much of this material fell relatively close to the crater, though significant amounts were emplaced as far as 4000 km from Chicxulub. For comparison the Toba volcanic eruption about 70,000 years ago is estimated to have released more than  $2 \times 10^{18}$  g of clastics (Matthews et al., 2012), a factor of about 15 less than our estimate for the Chicxulub impact in Table 1, but more than 200 times greater than the upper limit previously estimate by Pope (1997) for the clastics generated by Chicxulub.

The Toba eruption may have had a significant impact on the climate, as discussed further below; however, the magnitude of the effect is controversial. Alvarez et al. (1980), as well as Toon et al. (1982) and Pollack et al. (1983), thought that the K-Pg layer was dominated by submicron clastics that caused major loss of sunlight at the surface and consequently very low temperatures. However, while we don't know the fraction of the layer composed of submicron clastics, it is clear that the layer is both thinner than thought in the years just after its discovery and also dominated by other parts of the impact debris such as the spherules and the nano-particles. It would be very useful to measure the amount of submicron clastics in the K-Pg distal layer. Possibly, as suggested in Table 7, one could start by identifying the amount of submicron quartz in the layer by searching for small shocked quartz grains. Toon et al. (1997), and Pope (2002) used two differing indirect approaches to quantify the submicron clastics, and came up with answers that differ by a factor of about  $10^4$ . Here we attempted to reconcile these approaches, with the result shown in Table 1 yielding a significant optical depth. Although the submicron

clastics by themselves would have produced extreme climate changes if they were as abundant as we estimate, they would have been less important than the soot, and the nano-particles given our estimates here. The submicron clastics may have been injected higher than the soot, but lower than the nano-particles on average. Climate calculations involving all these materials are needed to understand how they may have interacted in the atmosphere.

The final particulates with large optical depths in Table 1 are sulfates. Pope et al. (1997), Pierazzo et al. (2003) and others have advocated for the importance of these particles in recent years. Unfortunately, sulfates in the K-Pg layer have not been traced unambiguously to the impact, because sulfur is so common in the environment. Possibly sulfur isotopic studies could distinguish the sulfur in the impactor from sulfur in the terrestrial environment, but we are not aware of such studies. While there is little doubt that large amounts of sulfur were present in the target material and in the asteroid, it is possible that much of it reacted with the hot rock in the impact plume, or the atmospheric layer heated by re-entering material. Sulfur is present in impact melt spherules and in carbonaceous clastics, so not all of it was released to the gas phase. Given the large opacity of the numerous types of particles in the atmosphere, photochemical reactions would have been inhibited, which would retard the conversion of sulfur dioxide gas into sulfate particles. It is possible that measurements of the sulfur mass independent fractionation (MIF) could reveal whether the sulfur quickly reacted with rocks, which should yield a MIF of zero, or if the sulfur slowly converted to sulfate, which might lead to MIF not being zero if resolved over the thickness of the distal layer. It is known that a non-zero MIF can occur following volcanic eruptions due to time dependent movement of sulfur between changing sulfur reservoirs in the atmosphere (e.g. Pavlov et al., 2005).

It is not clear if  $\text{SO}_3$  or  $\text{SO}_2$  was the dominant sulfur bearing gas in the ejecta plume. However, the gas phase reaction of  $\text{SO}_3$  and water is not a simple reaction as often abbreviated in papers about atmospheric sulfur chemistry, but instead involves water vapor clusters or  $\text{SO}_3$  adducts. Sulfur dioxide is observed to convert to particulates with an e-folding time of less than one month for moderate-sized volcanic eruptions such as the Mt. Pinatubo eruption. Following the K-Pg impact sulfur dioxide or trioxide gas may have had an extended lifetime in the atmosphere, due to the lack of sunlight to drive chemical reactions to convert it to sulfates. Clastics and nano-particles and soot, may have coagulated to large sizes and fallen out over a year or two. Alternatively, the sulfur gases may have reacted quickly on all the surfaces present, particularly in hot water present in the hot radiating layer when the ejecta reentered. Pope et al. (1997) and Pierazzo et al. (2003) have pointed out the possible importance of the extended lifetime of the sulfate to causing a prolonged period without photosynthesis in the oceans. However, clastics or soot need to be present in the sulfate to achieve the loss of sunlight. Recent work on the Toba eruption (Timmreck et al., 2010) shows that large sulfur injections do not produce proportionately larger climate perturbations because the climate effects of sulfur injections are self-limiting, as originally shown by Pinto et al. (1994) and recognized by Pope et al. (1997) and Pierazzo et al. (2003). Toba probably injected an amount of sulfur dioxide within an order of magnitude of that from the K-Pg impact. Larger particles have smaller optical depths, and shorter lifetimes, than smaller particles that result from smaller  $\text{SO}_2$  injections. Further work is needed to understand the

chemistry of the sulfur injected by the Chicxulub impact to determine if it was a significant factor in the extinction event.

Table 2 shows that significant injections of various ozone destroying chemicals such as NO<sub>x</sub>, Cl, Br, and I, likely occurred. The effects of these gases need to be considered in calculations but, given the expected darkness, photochemistry may have ceased until the atmosphere cleared.

Table 3 suggests that the much smaller mass injections from the impact of a 1 km diameter asteroid on land may produce optical depths that may still be important. Climate models are needed to fully evaluate these perturbations. At first glance the injections seem small. For example, the sulfur injection is only about 4 times larger than that from the Pinatubo eruption. However, the soot injection is very large. Robock et al. (2007a) and Mills et al. (2014) examined smoke injections at the tropopause of about one third the 1 km asteroid injection near the tropopause and found that the ozone layer was severely damaged, and low enough temperatures resulted to damage crops for a decade after the injection. Table 4 also indicates significant injections of iodine, which may further damage the ozone layer.

About 50 1-km impacts might have occurred since the demise of the dinosaurs. Based on the fraction of Earth covered by water, about 35 of these would be expected to have hit the oceans, perhaps resulting in large ozone losses as discussed by Pierazzo et al. (2010). Each of the 15 impacts that occurred on land might have led to significant injections of nano-particles. Paquay et al. (2008) recognized the osmium signature of two large impacts in the Late Eocene, which produce the 100 km diameter craters at Popigai and Chesapeake Bay. The osmium indicates a substantial input of vaporized impactor to the atmosphere from collisions of asteroids larger than 1 km in diameter. Climate model simulations are needed to evaluate the climate changes that might have occurred. The effects could have been variable for a variety of reasons, including variability in the light absorbing properties of rock from differing objects. To have injected significant amounts of smoke the impactor would need to hit a tropical forest, or at least a heavily forested region. About 26% of the world is currently forested; about 6% is in tropical rain forest. Forested area has greatly declined. Tropical rainforests might have covered as much as 20% of the Earth until recently. Hence, about 3 1-km objects might have hit a tropical rainforest and injected significant amounts of smoke since the K-Pg event.

In this work we have established a set of initial conditions (Tables 1-4) that may be used for modeling the climate and air chemistry after the K-Pg impact, or the impact of a 1 km asteroid. Other authors have considered some of these initial conditions, but some, such as the nano-particles from the vaporized impactor, have not been previously studied in the detail needed to fully evaluate their importance. Much more work is needed to obtain field data to further constrain some of parameters, and to resolve remaining differences of opinion about some of the values. However, simulations using these initial conditions can now be conducted with modern models of climate and atmospheric chemistry, which should shed light on the environmental conditions at the K-Pg boundary and the dangers posed by future impacts. We recently completed such simulations using the Whole Atmosphere Community Climate Model (WACCM) at the National Center for Atmospheric Research in a configuration similar to that used by Bardeen et al. (2008) and Mills et al. (2014).

**Author contributions:** Owen Toon worked to compile the particle and gas emissions. Charles Bardeen tested them in a climate model to determine if the initial conditions were specified completely. Rolando Garcia considered the gases that would be important for atmospheric chemistry.

**Acknowledgements:** We thank Wendy Wolbach for helpful comments about soot, and Brandon Johnson for helpful comments about nano-particles and spherules. C. Bardeen and R. Garcia were funded by NASA Exobiology grant #08-EXOB08-0016. The University of Colorado supported O. B. Toon's work.

## References

- Ahrens, T. J., and O'Keefe, J. D.: Impact of an asteroid or comet in the ocean and extinction of terrestrial life, *Proc. Lunar Planet. Sci. Conf.*, 13th, Part 2, *J. Geophys. Res.*, 88, suppl., A799–A806, 1983.
- Alvarez, L., Alvarez, W., Asaro, F. and Michel, H. V.: Extraterrestrial cause for the Cretaceous-Tertiary extinction, *Science*, 208, 1095–1108, 1980.
- Andreae, M. O. and Merlet, P.: Emission of trace gases and aerosols from biomass burning, *Global Biogeochem. Cycles*, 15, 955–966, 2001.
- Artemieva, N. and J. Morgan, J.: Modeling the formation of the K-Pg boundary layer, *Icarus*, 201, 768–780, 2009.
- Bardeen, C. G., Toon, O.B., Jensen, E.J., Marsh, D.R. and Harvey, V.L.: Numerical simulations of the three-dimensional distribution of meteoric dust in the mesosphere and upper stratosphere, *J. Geophys. Res.*, 113, D17202, doi:10.1029/2007JD009515, 2008.
- Belcher, C.M.: Reigniting the Cretaceous-Paleogene firestorm debate: *Geology*, 37, 1147–1148, doi: 10.1130/focus122009.1, 2009.
- Belcher, C.M., Collinson, M.E., Sweet, A.R., Hildebrand, A.R. and Scott, A.C.: Fireball passes and nothing burns—The role of thermal radiation in the Cretaceous–Tertiary event: Evidence from the charcoal record of North America: *Geology*, 31, 1061–1064, doi: 10.1130/G19989.1, 2003.
- Belcher, C.M., Collinson, M.E., Sweet, A.R., Hildebrand, A.R. and Scott, A.C.: Reply to Comment “Fireball passes and nothing burns. The role of thermal radiation in the K/T event: Evidence from the charcoal record of North America”, *Geology*, Online forum, 2004.
- Belcher, C.M., Collinson, M.E. and Scott, A.C.: Constraints on the thermal energy released from the Chicxulub impactor: New evidence from multimethod charcoal analysis: *Geological Society [London] Journal*, 162, 591–602, doi: 10.1144/0016-764904-104, 2005.
- Belcher, C.M., Finch, P., Collinson, M.E., Scott, A.C. and Grassineau, N.V.: Geochemical evidence for combustion of hydrocarbons during the K-T impact event: *National Academy of Sciences Proceedings*, 106, 4112–4117, doi: 10.1073/pnas.0813117106, 2009.
- Berndt, J., Deutsch, A., Schulte, P. and Mezger, K.: The Chicxulub ejecta deposit at Demerara Rise (western Atlantic): Dissecting the geochemical anomaly using laser ablation-mass spectrometry, *Geology*, 39, 279–282, 2011.
- Bhandari, N., Verma, H. C., Upadhyay, C., Tripathi, A. and Tripathi, R. P.: Global occurrence of magnetic and superparamagnetic iron phases in Cretaceous-Tertiary boundary clays, *Geolog. Soc. Am. Special Paper 356, Catastrophic Events and Mass Extinctions: Impacts and Beyond*, C. Koeberl and K. G. MacLleod eds., 2002.
- Birks, J. W., Crutzen, P. J., and Roble, R. G.: Frequent ozone depletion resulting from

1510 impacts of asteroids and comets. In Bobrowsky, P., Rickman, H. (Eds).  
1511 Comet/Asteroid Impacts and Human Society, Springer Pub., Berlin, 225-245, 2007.

1512 Bond, T. C. and Bergstrom, R. W.: Light absorption by carbonaceous particles: An  
1513 investigative review, *Aerosols Sci. Tech.*, 40, 27-67, 2006.

1514 Bohor, B.F.: Shock-induced microdeformations in quartz and other mineralogical  
1515 indications of an impact event at the Cretaceous-Tertiary boundary: Tectonophysics,  
1516 171, 359–372, doi: 10.1016/0040-1951(90)90110-T,1990.

1517 Bohor, B. F, Triplehorn, D. M., Nichols, D. J. and Millard, Jr., H. T.: Dinosaurs,  
1518 spherules, and the “magic layer”: A new K-T boundary clay site in Wyoming,  
1519 *Geology*, 15, 896-899, 1987.

1520 Bohor, B. F. and Glass, B. P.: Origin and diagenesis of K/T impact spherules-From Haiti  
1521 to Wyoming and beyond, *Meteoritics* 30, 182-198, 1995.

1522 Bosch, H., Camy-Peyret, C., Chipperfield, M. P., Fitzenberger, R., Harder, H., Platt, U.  
1523 and Pfeilsticker, K.: Upper limits of stratospheric IO and OIO inferred from center-to-  
1524 limb-darkening-corrected balloon-borne solar occultation visible spectra:  
1525 Implications for total gaseous iodine and stratospheric ozone, *J. Geophys. Res.*, 108,  
1526 D15,4455, doi:10.1029/2002JD003078, 2003.

1527 Boslough, M.B. and Crawford, D. A.: *Annals New York Acad. Sci.*, 822, 236-282,  
1528 doi: 10.1111/j.1749-6632.1997.tb48345, 1997.

1529 Ciais, P., et al.: Carbon and Other Biogeochemical Cycles, in *Climate Change 2013: The*  
1530 *Physical Science Basis. Contribution of Working Group I to the Fifth Assessment*  
1531 *Report of the Intergovernmental Panel on Climate Change* (Stocker et al. eds.)  
1532 Cambridge University Press, Cambridge, United Kingdom and New York, N.Y.,  
1533 USA, 2013.

1534 Crutzen, P. J., Galbally, I. E. and Brühl, C.: Atmospheric effects from post-nuclear fires,  
1535 *Climate Change*, 6, 323-364, 1984.

1536 Dorf, M., Butler, J. H., Butz, A., Camy-Peyret, C., Chipperfield, M. P., Kritten, L.,  
1537 Montzka, S. A., Simmes, B., Weidner, F. and Pfeilsticker, K.: Long-term  
1538 observations of stratospheric bromine, *Geophys. Res. Lett.*, 33, L24803,  
1539 doi:10.1029/2006GL027714, 2006.

1540 Durant, A. J., Rose, W. I., Sarna-Wojcicki, A. M., Carey, S. and Volentik, A. C. M.:  
1541 Hydrometeor-enhanced tephra sedimentation: Constraints from the 18 May 1980  
1542 eruption of Mount St. Helens, *J. Geophys. Res.* 114, B03204,  
1543 doi:10.1029/2008JB005756, 2009.

1544 Ferrow, E., Vajda, V., Koch, C. B., Peucker-Ehrenbrink, B., and Willumsen, P. S.:  
1545 Multiproxy analysis of a new terrestrial and a marine Cretaceous-Paleogene (K-Pg)  
1546 boundary site from New Zealand, *Geochim. et Cosmochim. Acta*, 75, 657-672, 2011.

1547 Folch, A., Costa, A., Durant, A. and Macedonio, G.: A model for wet aggregation of ash  
1548 particles in volcanic plumes and clouds: 2. Model application, *J. Geophys. Res.*, 115,  
1549 B09202, doi10.1029/2009JB007176, 2010.

1550 Glass B. P. and Simonson B. M.: Distal impact ejecta layers: spherules and more.

1551 Elements 8, 43–48, 2012.

1552 Goldin, T.J., and Melosh, H.J.: Self-shielding of thermal radiation by Chicxulub impact  
1553 ejecta: Firestorm or fizzle?: *Geology*, 37, 1135–1138, doi: 10.1130/G30433A.1, 2009.

1554 Goles, G. G., Greenland L. P. and Jerome, D. Y.: Abundances of chlorine, bromine and  
1555 iodine in meteorites, *Geochim. Cosmochim. Acta*, 31, 1771–1787, 1967.

1556 Guo, S., Bluth, G. J. S., Rose, W. I., Watson, I. M. and Prata, A. J.: Re-evaluation of SO<sub>2</sub>  
1557 release of the 15 June 1991 Pinatubo eruption using ultraviolet and infrared satellite  
1558 sensors, *Geochem. Geophys. Geosyst.*, 5, Q04001, doi:10.1029/ 2003GC000654,  
1559 2004.

1560 Harvey, M.C., Brassell, S.C., Belcher, C.M., and Montanari, A.: Combustion of fossil  
1561 organic matter at the Cretaceous–Paleogene (K–P) boundary, *Geology*, 36, 355–358,  
1562 doi:10.1130/G24646A.1, 2008.

1563 Hervig, M. E., Gordley, L. L., Deaver, L. E., Siskind, D. E., Stevens, M. H., Russell III,  
1564 J. M., Bailey, S. M., Megner, L. and C. G. Bardeen.: First Satellite Observations of  
1565 Meteoric Smoke in the Middle Atmosphere, *Geophys. Res. Lett.*, 36, L18805,  
1566 doi:10.1029/2009GL039737, 2009.

1567 Hildebrand, A. R.: The Cretaceous/Tertiary boundary impact (or the dinosaurs didn't  
1568 have a chance), *J. Roy. Astron. Soc. Can.*, 87, 77–118, 1993.

1569 Houghton, R. A.: Above ground forest biomass and the global carbon balance, *Global  
1570 Change Biology*, 11, 945–958, 2005.

1571 Hunten, D. M., Turco, R. P., and Toon, O. B.: Smoke and dust particles of meteoric  
1572 origin in the mesosphere and stratosphere, *J. Atmos. Sci.*, 37, 1342–1357, 1980.

1573 Ivany, L.C. and Salawitch, R. J.: Carbon isotopic evidence for biomass burning at the K-  
1574 T boundary, *Geology*, 21, 487–490, 1993.

1575 Johnson, B.C. and Bowling, T. J.: Where have all the craters gone? Earth's  
1576 bombardment history and the expected terrestrial cratering record, *Geology* 42, 587-  
1577 590, 2014.

1578 Johnson B. C. and Melosh H. J.: Impact spherules as a record of an ancient heavy  
1579 bombardment of Earth, *Nature* 485, 75–77, 2012a.

1580 Johnson, B. C., and Melosh, H. J.: Formation of spherules in impact produced vapor  
1581 plumes, *Icarus*, 217, 416–430, 2012b.

1582 Johnson, B. C., and Melosh, H. J.: Formation of melt droplets, melt fragments, and  
1583 accretionary impact lapilli during hypervelocity impact, *Icarus*, 228, 347–363, 2014.

1584 Jones, E. M. and Kodis, J. W.: Atmospheric effects of large body impacts: The first few  
1585 minutes, in *Geological Implications of Impacts of Large Asteroids and Comets on the  
1586 Earth*, edited by L. T. Silver and P. H. Schultz, *Geol. Soc. Am. Special Paper* 190,  
1587 175–186, 1982.

1588 Kaiho, K., et al.: Global climate change driven by soot at the K-Pg boundary as the cause  
1589 of the mass extinction, *Sci. Rep.* 6, 28427; doi: 10.1038/srep28427, 2016.

1590 Kalashnikova, O., Horanyi, M., Thomas, G. E. and Toon, O. B.: Meteoric smoke  
1591 production in the atmosphere, *Geophys. Res. Lett.*, 27, 3293-3296, 2000.

1592 Kallemeyn, G. W. and Wasson, J. T.: The compositional classification of chondrites-I.  
1593 The carbonaceous chondrite groups, *Geochim. Cosmochim. Acta* 45, 1217-1230,  
1594 1981.

1595 Kring, D. A., and Durda, D. D.: Trajectories and distribution of material ejected from the  
1596 Chicxulub impact crater: Implications for post impact wildfires, *J. Geophys. Res.*,  
1597 107, E8, 5062, 10.1029/2001JE001532, 2002.

1598 Kring, D. A., Melosh, H. J. and Hunten, D. M.: Impact-induced perturbations of  
1599 atmospheric sulfur, *Earth Planet. Sci. Lett.*, 14, 201-212, 1996.

1600 Lack, D. A., Bahreini, R., Cappa, C. D., Middlebrook, A. M. and Schwartz, J. P.: Brown  
1601 carbon and internal mixing in biomass burning particles, *Pub. Nat. Acad. Sci.*, 109,  
1602 14802-14807, 2012.

1603 Malone, R. C., Auer, L., Glatzmaier, G., Wood, M. and Toon, O. B.: Influence of Solar  
1604 Heating and Precipitation Scavenging on the Simulated Lifetime of Post-Nuclear War  
1605 Smoke, *Science*, 230, 317-319, 1985.

1606 Matichuk, R. I., Colarco, P.R., Smith, J.A. and Toon, O.B.: Modeling the transport and  
1607 optical properties of smoke plumes from South American biomass burning, *J.*  
1608 *Geophys. Res.*, 113, D07208, doi:10.1029/2007JD009005, 2008.

1609 Matthews, N. E., Smith, V. C., Costa, A., Durant, A J., Pyle, D. M. and Pearce, N. J. G.:  
1610 Ultra-distal tephra deposits from super-eruptions: Examples from Toba, Indonesia  
1611 and Taupo Volcanic Zone, New Zealand, *Quaternary Int.* 258, 54-79, 2012.

1612 Melosh, H.J. and Vickery, A.M.: Melt droplet formation in energetic impact events,  
1613 *Nature* 350, 494–497, 1991.

1614 Melosh, H.J., Schneider, N.M., Zahnle, K.J. and Latham, D.: Ignition of global wildfires  
1615 at the Cretaceous–Tertiary boundary, *Nature*, 343, 251–254, 1990.

1616 Mikhailov, E. F., Vlasenko, S. S., Podgorny, I. A., Ramanathan, V., Corrigan, C. E.:  
1617 Optical properties of soot-water drop agglomerates: An experimental study, *J.*  
1618 *Geophys. Res.*, 111, D07209, doi:10.1029/2005JD006389, 2006.

1619 Millero, F. J., Feistel, R., Wright, D. G. and McDougall, T. J.: The composition of  
1620 standard seawater and the definition of the reference composition salinity scale,  
1621 *Deep-Sea Res.*, 55, 50-72, 2008.

1622 Mills, M. J., Toon, O. B., Turco, R.P., Kinnison, D.E. and Garcia, R.R.: Massive global  
1623 ozone loss predicted following regional nuclear conflict, *P. Nat. Acad. Sci.*, 105,  
1624 5307-5312, 2008.

1625 Mills, M. J., Toon, O. B. and Robock, A.: Multidecadal global cooling and unprecedented  
1626 ozone loss following a regional nuclear conflict, *Earth's Future*, 2, 161-176,  
1627 doi:10.1002/2013EF00020, 2014.

1628 Milne, P. H. and McKay, C.: Response of marine plankton communities to a global  
1629 atmospheric darkening, in *Geological Implications of Impacts of Large Asteroids and*

- 1630 Comets on the Earth, edited by L. T. Silver and P. H. Schultz, Geol. Soc. Am. Special  
1631 Paper 190, 297-303, 1982.
- 1632 Morgan, J., Artemieva, N., and Goldin, T.: Revisiting wildfires at the K-Pg boundary, J.  
1633 Geophys. Res. Biogeosci., 118, 1-13, doi:10.1002/2013JG002428, 2013.
- 1634 Nassar, R., et al.: A global inventory of stratospheric chlorine in 2004, J. Geophys. Res.,  
1635 111, D22312, doi:10.1029/2006JD007073, 2006.
- 1636 Neely, R., English, J. M., Toon, O. B., Solomon, S., Mills, M. and Thayer, J. P.:  
1637 Implications of extinction due to meteoritic smoke in the upper stratosphere,  
1638 Geophys. Res. Lett., 38 L24808, doi 10.1029/2011GL049865, 2011.
- 1639 O’Keefe, J.D. and Ahrens, T.J.: The interaction of the Cretaceous/Tertiary Extinction  
1640 Bolide with the atmosphere, ocean, and solid Earth, in Geological Implications of  
1641 Impacts of Large Asteroids and Comets on the Earth, edited by L. T. Silver and P. H.  
1642 Schultz, Geol. Soc. Am. Spec. Pap. 190, 103–120, 1982.
- 1643 Orofino, V., Blanco, A., Fonti, S., Proce, R. and Rotundi, A.: The infrared optical  
1644 constants of limestone particles and implications for the search of carbonates on  
1645 Mars, Planet. Space Sci., 46, 1659-1669, 1998.
- 1646 Pan, Y., et al.: A large and persistent carbon sink in the world’s forests, Science, 333,  
1647 988-993, 2011.
- 1648 Paquay F. S., Ravizza G. E., Dalai T. K. and Peucker-Ehrenbrink B.: Determining  
1649 chondritic impactor size from the marine osmium isotope record. Science 320, 214–  
1650 218, 2008.
- 1651 Parkos, D., Alexeenko, A., Kulakhmetov, M., Johnson, B. C., and Melosh, H. J.: NOx  
1652 production and rainout from Chicxulub impact ejecta and reentry, J. Geophys. Res. –  
1653 Planets, 120, doi 10.1002/2015JE004857, 2015.
- 1654 Pavlov, A.A., Mills, M.J. and Toon, O. B.: Mystery of the volcanic mass-independent  
1655 sulfur isotope fractionation signature in the Antarctic ice-core, Geophys. Res. Lett.,  
1656 32, L12816, doi:10.1029/2005GL022784, 2005.
- 1657 Penner, J. E., Haselman, Jr., L.C. and Edwards, L. L.: Smoke-plume distributions above  
1658 large-scale fires: Implications for simulations of “Nuclear Winter”, J. Climate and  
1659 Appl. Meteor., 25, 1434-1444, 1986.
- 1660 Pierazzo, E., Hahmann, A. N. and Sloan, L.C.: Chicxulub and climate: Radiative  
1661 perturbations of impact-produced S-bearing gases, Astrobio., 3, 99-118, 2003.
- 1662 Pierazzo, E., Garcia, R. R., Kinnison, D. E., Marsh, D. R., Lee-Taylor, J. and Crutzen, P.  
1663 J.: Ozone perturbation from medium-sized asteroid impacts in the ocean, Earth and  
1664 Planet Sci. Lett., doi:10.1016/j.epsl.2010.08.036, 2010.
- 1665 Pierazzo, E. and Artemieva, N.: Local and global environmental effects of impacts on  
1666 Earth, Elements, 8, 55-60, 2012.
- 1667 Pittock, A. B., Ackerman, T. P., Crutzen, P. J., MacCracken, M. C., Shapiro, C. S., and  
1668 Turco, R. P.: Environmental Consequences of Nuclear War SCOPE-28, Vol. 1,  
1669 Physical and Atmospheric Effects, Wiley, Chichester, England, 1985 (Second ed.

1670 1989).

1671 Pinto J.R., Turco R.P., Toon, O.B.: Self-limiting physical and chemical effects in  
 1672 volcanic eruption clouds, *J. Geophys. Res.*, 94, 11165–11174, doi:10.1029/  
 1673 JD094iD08p11165, 1989.

1674 Pollack, J.B., Toon, O. B., Ackerman, T. P., McKay, C. P. and Turco, R. P.:  
 1675 Environmental effects of an impact generated dust cloud: Implications for the  
 1676 Cretaceous-Tertiary extinctions, *Science*, 219, 287-289, 1983.

1677 Pope, K. O.: Impact dust not the cause of the Cretaceous-Tertiary mass extinction,  
 1678 *Geology*, 30, 99-102, 2002.

1679 Pope, K. O., Baines, K. H., Ocampo, A. C. and Ivanov, B. A.: Energy, volatile  
 1680 production, and climatic effects of the Chicxulub Cretaceous/Tertiary impact, *J.*  
 1681 *Geophys. Res.*, 102, 21645-21664, 1997.

1682 Premovic', P. I.: Soot in Cretaceous-Paleogene boundary clays worldwide: Is it really  
 1683 derived from fossil fuel beds close to Chicxulub?, *Centra. European J. Geosci.*, 4,  
 1684 383-387, 2012.

1685 Pueschel, R. F., Russell, P. B., Allen, D. A., Ferry, G. V., Snetsinger, K. G., Livingston,  
 1686 K. G. and Verma, S.: Physical and optical properties of the Pinatubo volcanic aerosol:  
 1687 Aircraft observations with impactors and a Sun-tracking photometer, *J. Geophys.*  
 1688 *Res.*, 99, 12,915-12,922, 1994.

1689 Querry, M. R., Osborne, G., Lies, K., Jordon, R. and Covey, R. M.: Complex refractive  
 1690 index of limestone in the visible and infrared, *Applied Optics*, 17, 353-356, 1978.

1691 Renne, P. R., et al.: Time scales of critical events around the Cretaceous-Paleogene  
 1692 boundary, *Science*, 339, 684-687, 2013.

1693 Robertson, D.S., McKenna, M.C., Toon, O.B., Hope, S. and Lillegraven, J.A.: Survival in  
 1694 the first hours of the Cenozoic: *Geological Society of America Bulletin*, 116, 760–  
 1695 768, doi: 10.1120/B25402.1, 2004.

1696 Robertson, D. S., Lewis, W. M., Sheehan, P. M. and Toon, O. B.: K-Pg extinction:  
 1697 Reevaluation of the heat-fire hypothesis, *J. Geophys. Res.*, 118, 329-336,  
 1698 doi10.1002/jgrg.20018, 2013a.

1699 Robertson, D. S., Lewis, W. M., Sheehan, P. M. and Toon, O. B.: K-Pg extinction  
 1700 patterns in marine and freshwater environments: The impact winter model, *J.*  
 1701 *Geophys. Res.*, 118, 1006-1014, doi10.1002/jgrg.20086, 2013b.

1702 Robock, A., Oman, L., Stenchikov, G.L., Toon, O. B., Bardeen, C. and Turco, R.P.:  
 1703 Climatic consequences of regional nuclear conflicts, *Atmos. Chem. Phys.* 7, 1973-  
 1704 2002, 2007a.

1705 Robock, A., Oman, L., and Stenchikov, G. L.: Nuclear winter revisited with a modern  
 1706 climate model and current nuclear arsenals: Still catastrophic consequences, *J.*  
 1707 *Geophys. Res.*, 112, D13107, doi:10.1029/2006JD008235, 2007b.

1708 Rose, W. I. and Durant, A. J.: Fine ash content of explosive eruptions, *J. Volcan.*  
 1709 *Geothermal Res.*, 186, 32-39, 2009.

- 1710 Schmidt, A., et al.: Selective environmental stress from sulfur emitted by continental  
1711 flood basalt eruptions, *Nature Geosci.*, 9, 77-82, 2016.
- 1712 Schulte, P., Deutsch, A., Salge, T., Berndt, J., Kontny, A., MacLeod, K. G., Neuser, R. D.  
1713 and Krumm, S.: *Geochim. Cosmochim. Acta*, 73, 1180-1204, 2008.
- 1714 Schulte, P. et al.: The Chicxulub Asteroid Impact and Mass Extinction at the Cretaceous-  
1715 Paleogene Boundary, *Science*, 327, 1214-1218, doi: 10.1126/science.1177265, 2010.
- 1716 Small, R. D. and Heikes, K. E.: Early cloud formation and large area fires, *J. Appl.*  
1717 *Meteorol.*, 27, 654-663, 1988.
- 1718 Smit, J.: The global stratigraphy of the Cretaceous-Tertiary boundary impact ejecta, *Ann.*  
1719 *Rev. Earth Planet. Sci.*, 27, 75-113, 1999.
- 1720 Stothers, R. B.: The great Tambora eruption in 1815 and its aftermath, *Science*, 224,  
1721 1191-1198, 1984.
- 1722 Timmreck C., Graf, H. F., Lorenz, S. J., Niemeier, U., Zanchettin, D., Matei, D.,  
1723 Jungclaus, J. H., Crowley, T.J.: Aerosol size confines climate response to volcanic  
1724 super-eruptions, *Geophys. Res. Lett.*, 37, L24705, doi:10.1029/2010GL045464, 2010.
- 1725 Toon, O. B., and Ackerman, T. P.: Algorithms for the Calculation of Scattering by  
1726 Stratified Spheres, *Appl. Optics*, 20, 3657-3660, 1981.
- 1727 Toon, O. B., Pollack, J. B., Ackerman, T.P., Turco, R.P., McKay, C.P. and Liu, M.S.:  
1728 Evolution of an Impact-Generated Dust Cloud and its Effects on the Atmosphere, in  
1729 *Geological Implications of Impacts of Large Asteroids and Comets on the Earth*,  
1730 edited by L. T. Silver and P. H. Schultz, *Geological Soc. Am. Spec. Paper* 190, 187-  
1731 200, 1982.
- 1732 Toon, O. B., Zahnle, K., Morrison, D., Turco, R. P. and Covey, C.: Environmental  
1733 perturbations caused by the impacts of asteroids and comets: *Reviews of Geophysics*,  
1734 35, 41-78, 1997.
- 1735 Toon, O. B., Turco, R. P., Robock, A., Bardeen, C., Oman, L. and Stenchikov, G. L.,  
1736 Atmospheric effects and societal consequences of regional scale nuclear conflicts and  
1737 acts of individual nuclear terrorism, *Atmos. Chem. Phys.*, 7, 1973-2002, 2007.
- 1738 Trinquier, A., Birck, J. -L., Alle`gre, C. J.: The nature of the KT impactor. A  $^{54}\text{Cr}$   
1739 reappraisal, *Earth and Planet. Sci. Lett.*, 241, 780-788, 2006.
- 1740 Turco, R. P., Toon, O. B., Whitten, R. C., Hamill, P., and Keesee, R. G.: The 1980  
1741 eruptions of Mt. St. Helens: Physical and chemical processes in stratospheric clouds,  
1742 *J. Geophys. Res.*, 88, 5299-5319, 1983.
- 1743 Turco, R. P., Toon, O. B., Ackerman, T. P., Pollack, J.B. and Sagan, C.: Climate and  
1744 smoke: An appraisal of nuclear winter, *Science*, 247, 166-176, 1990.
- 1745 Verma, H. C., Upadhyay, C., Tripathi, A., Tripathi, R. P. T. and Bhandari, N.: Thermal  
1746 decomposition pattern and particle size estimate of iron minerals associated with the  
1747 Cretaceous-Tertiary boundary at Gubbio, *Meteor. Planet. Sci.*, 37, 901-909, 2002.
- 1748 Vajda, V., Ocampo, A., Ferrow, E., Koch, C. B.: Nano-particles as the primary cause of  
1749 long-term sunlight suppression at high latitudes following the Chicxulub impact-

1750 evidence from ejecta deposits in Belize and Mexico, *Godwana Res.*, 27, 1079-1088,  
1751 2015.

1752 Ward, W. C., Keller, G., Stinnesbeck, W., and Adatte, T.: Yucatan subsurface  
1753 stratigraphy: Implications and constraints for the Chicxulub impact, *Geology*, 23,  
1754 873-876, 1995.

1755 Wdowiak, T. J., Armendarez, L. P., Agresti, D. G., Wade, M. L., Wdowiak, S. Y.,  
1756 Claeys, P. and Izett, G.: Presence of an iron-rich nanophase material in the upper  
1757 layer of the Cretaceous-Tertiary boundary clay, *Meteoritics Planet. Sci.*, 36, 123-133,  
1758 2001.

1759 Wolbach, W.S., Lewis, R.S. and Anders, E.: Cretaceous extinctions: Evidence for  
1760 wildfires and search for meteoritic material, *Science*, 240, 167-170, 1985.

1761 Wolbach, W.S., Gilmour, I., Anders, E., Orth, C.J. and Brooks, R.R.: Global fire at the  
1762 Cretaceous-Tertiary boundary, *Nature*, 334, 665-669, 1988.

1763 Wolbach, W.S., Anders, E. and Nazarov, M. A.: Fires at the K-T Boundary: Carbon at  
1764 the Sumbar, Turkmenia site, *Geochemica et Cosmochimica Acta*, 54, 1133-1146.  
1765 1990a.

1766 Wolbach, W. S., Gilmour, I. and Anders E.: Major wildfires at the Cretaceous/Tertiary  
1767 boundary, in *Global Catastrophes in Earth History: An Interdisciplinary Conference*  
1768 *on Impacts, Volcanism and Mass Mortality*, ed. Sharpton, V.L. and Ward, P. D.,  
1769 *Geological. Soc. Am. Spec. Paper* 247, 391-400, 1990b.

1770 Wolbach, W. S., Widicus, S. and Kyte, F. T.: A search for soot from global wildfires in  
1771 Central Pacific Cretaceous-Tertiary boundary and other extinction and impact horizon  
1772 sediments, *Astrobio.*, 3, 91-97, 2003.

1773 Wolf, E. T. and Toon, O. B.: Fractal organic hazes provide an ultraviolet shield for early  
1774 Earth, *Science*, 328, 1266-1268, 2010.

1775 Yancy, T. and Guillemette, R. N.: Carbonate accretionary lapilli in distal deposits of the  
1776 Chicxulub impact event, *Geolog. Soc. Am. Bull.*, 120, 1105-1118, 2008.

1777 Zahnle, K.: Atmospheric chemistry by large impacts, in *Global Catastrophes in Earth*  
1778 *History: An Interdisciplinary Conference on Impacts, Volcanism and Mass Mortality*,  
1779 ed. Sharpton, V.L. and Ward, P. D., *Geological. Soc. Am. Spec. Paper* 247, 271-288,  
1780 1990.  
1781

1782 Table 1: K-Pg injection scenario for impactor mass  $\sim 1.4 \times 10^{18}$  g, impact energy  $\sim 2.8 \times 10^{23}$   
1783  $J = 6.8 \times 10^7$  Mt for 20 km/s impact

Property/ Constituent	Type 2 spherules	Soot	Nano- particles	Clastics, < $\mu\text{m}$	S
Material amount, g, column density (g $\text{cm}^{-2}$ )	$2.3 \times 10^{18}$ (0.44)	$1.5\text{-}5.6 \times 10^{16}$ (0.29 to $1.1 \times 10^{-2}$ ) <sup>***</sup>	$\sim 2 \times 10^{18}$ <sup>**</sup> (0.4)	$< 6 \times 10^{16}$ (0.01)	$9 \times 10^{16}$ ( $5.4 \times 10^{-2}$ g $\text{SO}_4/\text{cm}^2$ )
Global optical depth as 1 $\mu\text{m}$ particles *	$\sim 20$ (for 250 $\mu\text{m}$ particles)	$\sim 100$	$\sim 2000$	$\sim 90$	$\sim 450$
Vertical distribution	70 km, Gaussian distribution with half width of 6.6 km <sup>****</sup>	Eq. 2	Same as Type 2 spherules	Uniformly mixed vertically above tropopause	Same as Type 2 spherules
Optical properties	Not relevant	$n=1.8$ $k=0.67$	Hervig et al., (2009)	Orofino et al. (1998) limestone	Sulfuric acid
Initial Particle size	250 $\mu\text{m}$ diameter	Lognormal, $r_m=0.11 \mu\text{m}$ , $\sigma=1.6$ ; monomers 30-60 nm	20 nm diameter	Lognormal, $r_m=0.5 \mu\text{m}$ , $\sigma=1.65$	gas
Material density, g $\text{cm}^{-3}$	2.7	1.8	2.7	2.7	1.8

1784 \*Qualitative estimate for comparison purposes only

1785 \*\*This value is an upper limit. The lower limit is zero

1786 \*\*\*These values are for aciniform soot, or elemental carbon in the stratosphere, see text.

1787 \*\*\*\*The material may have quickly moved to below 50 km to maintain hydrostatic  
1788 balance. See text.

1789

1790

1791 Table 2: Gas phase emissions (g) from the Chixculub impact

Sources/ Gases****	S ( $\times 10^{13}$ )	C (as $\text{CO}_2^{**}$ ) ( $\times 10^{17}$ )	$\text{H}_2\text{O}$ ( $\times 10^{15}$ )	Cl ( $\times 10^{12}$ )	Br ( $\times 10^{10}$ )	I ( $\times 10^7$ )	N ( $\times 10^{14}$ )	Vertical distribution
Ambient burden (g)	1*	8.4	1.3 strat	2.3 strat	3.1 strat	<2.3 strat	2 as $\text{N}_2\text{O}$	
Impactor	$4 \times 10^3$	0.3	200	$7 \times 10^2$	$5 \times 10^2$	$7 \times 10^4$		As Type 2 spherules
Forest fires	40	6	1500	200	1000	$9 \times 10^5$	10	As soot
Vaporized sea water	60	small	600	$1 \times 10^4$	$5 \times 10^3$	40	-	As Type 2 spherules
Splashed sea water***	500	small	$5 \times 10^3$	$1 \times 10^5$	$4 \times 10^4$	$3 \times 10^2$	-	Uniformly mixed above tropopause
Impact site (vaporized)	5000	0.6	90	800	400	3		As Type 2 spherules
Impact site (degassed)	500	0.1	120	$2 \times 10^3$	$1 \times 10^3$	7		Uniformly mixed above tropopause
Air heating							300 as $\text{NO}_x$ created from air	Half uniformly mixed, half as Type 2 spherules

1792 \* Based on Pinatubo eruption

1793 \*\* Mass is given in terms of C, but emission is in the form of  $\text{CO}_2$ 

1794 \*\*\* S, Cl, Br, I likely injected as particulates

1795 \*\*\*\* The scaling factors given in ( ) apply to all values in column.

1796

1797

1798 Table 3: 1 km land\* injection scenario for impactor mass  $1.4 \times 10^{15}$  g; impactor energy  
1799  $\sim 2.8 \times 10^{20}$  J =  $6.8 \times 10^4$  Mt

Property/ Constituent	Type 2 spherules	Soot**	Nano- particles from vaporized rock***	Clastics, $< \mu\text{m}$ distributed globally	S
Material amount g, column density ( $\text{g cm}^{-2}$ )	$1.4 \times 10^{15}$ ( $2.6 \times 10^{-4}$ )	$2.8 \times 10^{13}$ ( $5.6 \times 10^{-6}$ )	$1 \times 10^{15}$ ( $2 \times 10^{-4}$ )	$2.6 \times 10^{13}$ ( $5 \times 10^{-6}$ )	$4.4 \times 10^{13}$ ( $2.6 \times 10^{-5}$ g $\text{SO}_4 \text{ cm}^{-2}$ )
Estimated global optical depth as 1 $\mu\text{m}$ particles	0.2 (as 15 $\mu\text{m}$ particles)	$4.7 \times 10^{-2}$	1.5	$4 \times 10^{-2}$	0.22
Vertical & horizontal distributions	Table 1 Over 50% of Earth	50% Eq. 2+50% Eq 3 Over $4 \times 10^4$ $\text{km}^2$	Table 1 Over 50% of Earth	Uniformly mixed above tropopause, spread over $4 \times 10^5 \text{ km}^2$	Follow nano- particles
Optical properties	Not relevant	Table 1	Table 1	Depends on impact site	Table 1
Initial particle size ( $\mu\text{m}$ )	15 $\mu\text{m}$	Table 1	20 nm	Table 1	

1800 \*We assume a 1 km asteroid impact would not penetrate through the 5km average depth  
1801 of the ocean. Therefore, none of the materials in this Table would be injected into the  
1802 atmosphere for an ocean impact. For the density of all materials follow Table 1.

1803 \*\*The material amount assumes an impact into a region where  $2.25 \text{ g C cm}^{-2}$  flammable  
1804 biomass is consumed. The material amount can be scaled linearly for other choices of  
1805 available biomass that burns.

1806 \*\*\*We assume about 35% of the impactor and an equivalent mass of target would vaporize  
1807 and end up as nano-particles. This value is an upper limit. The lower limit is zero.

1808  
1809

1810 Table 4: Gas phase emissions (g) from a 1-km diameter impact

Sources/ Gases****	S ( $\times 10^{13}$ )	C* ( $\times 10^{17}$ )	H <sub>2</sub> O ( $\times 10^{15}$ )	Cl ( $\times 10^{12}$ )	Br ( $\times 10^{10}$ )	I ( $\times 10^7$ )	N ( $\times 10^{14}$ )	Vertical distribution
Ambient burden (g)	1**	8.4	1.3 strat	2.3 strat	3.1 strat	<2.3 strat	2 as N <sub>2</sub> O**	
Impactor/ land only	4.4	$3 \times 10^{-2}$	0.2	0.7	0.5	68	-	As type 2 spherules
Forest fires/land only	$2.7 \times 10^{-2}$	$4 \times 10^{-3}$	0.9	0.12	0.62	560	$6.9 \times 10^{-3}$	As soot
Vaporized sea water	0.9	small	10	200	80	0.6		Uniformly mixed
Splashed sea water***	3	small	30	600	200	2		
Air heating							0.6	Uniformly mixed

1811 \* mass is given in terms of C, but emission is in the form of CO<sub>2</sub>

1812 \*\*based on Pinatubo volcanic eruption

1813 \*\*\*S, Cl , Br, I may be released as particulates

1814 \*\*\*\* scaling factors given in ( ) apply to all values in column

1815

1816

1817 Table 5: Comparison of Toon et al. (1997) and Pope (2002) estimates of submicron  
1818 clastics.

Method	Quartz based estimate- Pope (2002)	Injected mass-Toon et al. (1997)*	Injected mass - revised	Quartz based estimate-revised	1 km impactor**
Initial clastic debris, g	$<10^{16}$	$7 \times 10^{20}$	$2.9 \times 10^{19}$	$5 \times 10^{18}$	$1.3 \times 10^{16}$
% clastic $<1 \mu\text{m}$	$<1$	0.1	2	1	2
Submicron clastics, g	$<10^{14}$	$7 \times 10^{17}$	$5.8 \times 10^{17}$	$5 \times 10^{16}$	$2.6 \times 10^{14}$
Stratospheric submicron surviving initial removal, g	$10^{14}$	$7 \times 10^{17}$	$<5.8 \times 10^{16}$	$5 \times 10^{16}$	$< 2.6 \times 10^{13}$

1819 \* assuming an impact energy of  $1.5 \times 10^8 \text{Mt}$ , and a velocity of 20 km/s.

1820 \*\* scaled from Injected Mass Revised using energy scaling assuming an impact energy of  
1821  $6.8 \times 10^4 \text{Mt}$

1822

1823

1824

1825 Table 6: Impactor composition, seawater composition, Yucatan impact site composition  
1826 and forest fire emission ratios

	S	C	H <sub>2</sub> O	Cl	Br	I	EC	N
Carbonaceous Chondrite (g/g impactor)	3.1 $\times 10^{-2}$	1.98 $\times 10^{-2}$	11.9 $\times 10^{-2}$	4.7 $\times 10^{-6}$	3.27 $\times 10^{-6}$	4.8 $\times 10^{-7}$		
Sea water (g/g sea water)	9.1 $\times 10^{-4}$	3 $\times 10^{-6}$	0.965	1.9 $\times 10^{-2}$	8.2 $\times 10^{-5}$	6.0 $\times 10^{-10}$	-	-
Impact site (g/g site)	7.1 $\times 10^{-2}$	9.6 $\times 10^{-2}$	0.07					
Emission ratios for forest fires g/g of dry biomass burned	2.9 $\times 10^{-4*}$	4.3 $\times 10^{-1}$ as CO <sub>2</sub> 4.4 $\times 10^{-2}$ as CO 5.1 $\times 10^{-3}$ as CH <sub>4</sub>	Highly variable, can equal dry weight	As CH <sub>3</sub> Cl 1.4 $\times 10^{-5}$ to 1.3 $\times 10^{-4}$	As CH <sub>3</sub> Br 6.7 $\times 10^{-6}$	As CH <sub>3</sub> I 6.1 $\times 10^{-6}$	6.6 $\times 10^{-4**}$	7.5 $\times 10^{-4}$ as NO 6 $\times 10^{-5}$ as N <sub>2</sub> O

1827 \*The mass is given in terms of S, but the emission is in the form of SO<sub>2</sub>.

1828 \*\* We used 0.03 g/g in Table 3, because forest fires will not produce as much soot as mass  
1829 fires.

1830

1831 Table 7 Suggestions for data collection

Property of interest	Rationale
Global distribution of spherules	Some impact models suggest spherules were not distributed globally, limiting area of Earth that might experience fire ignition
Number concentration, size of spherules	Current data are incomplete on number and size of spherules
Soot distribution	Profile soot/iridium/spherule distribution to determine if fires are contemporaneous with iridium fallout
Nano-meter material	Nano-meter material has been detected, but its mass needs to be quantified
Clastics	Submicron component not detected. Possibly search for micron/submicron shocked quartz.
Sulfur	Use sulfur isotopes to search for extraterrestrial sulfur, sulfur MIF to test for prolonged lifetime

1832

1833

Figure Captions

Figure 1. Injection profiles for smoke at midlatitudes and the tropics and for large spherical particles. Many other constituents follow the same vertical profiles as noted in Table 1-4. We suggested clastics be placed above the tropopause using a constant mixing ratio.

Figure 2. The size distributions for smoke from modern fires in Africa, and from the K-Pg boundary layer (Wolbach et al., 1985; Matichuk et al., 2008).

Figure 3. The real and imaginary parts of the refractive index suggested for nanoparticles, and for soot.

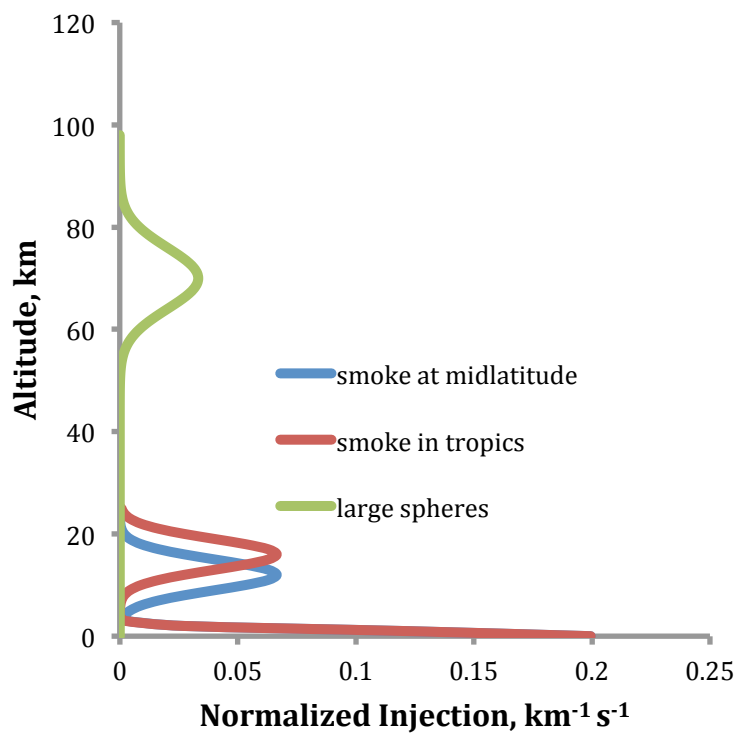


Figure 1. Injection profiles for smoke at midlatitudes and the tropics and for large spherical particles. Many other constituents follow the same vertical profiles as noted in Table 1-4. We suggested clastics be placed above the tropopause using a constant mixing ratio.

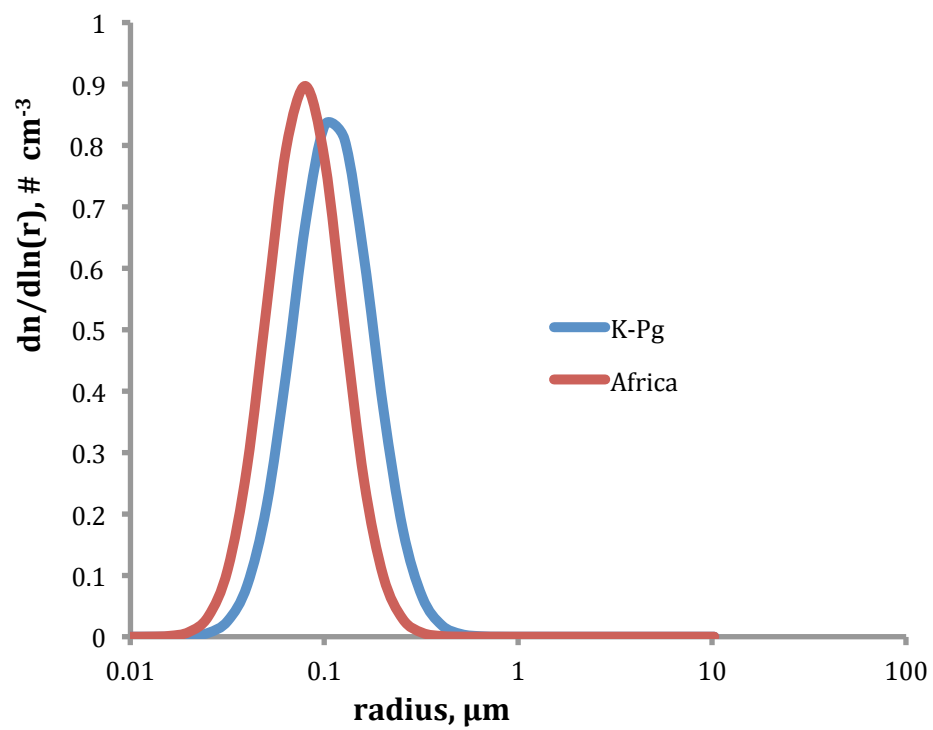


Fig. 2. The size distributions for smoke from modern fires in Africa, and from the K-Pg boundary layer (Wolbach et al., 1985; Matichuk et al., 2008)

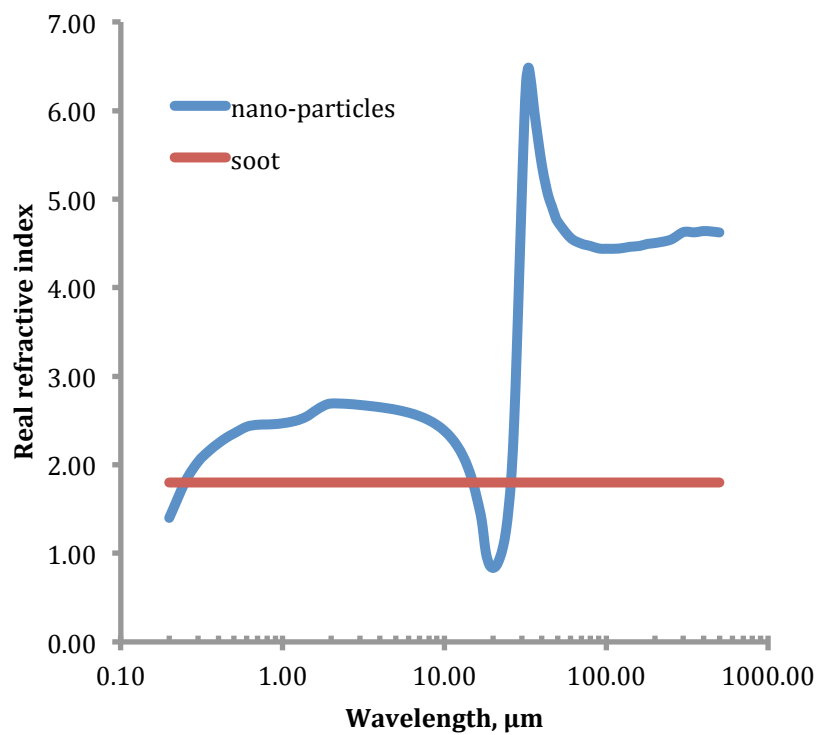
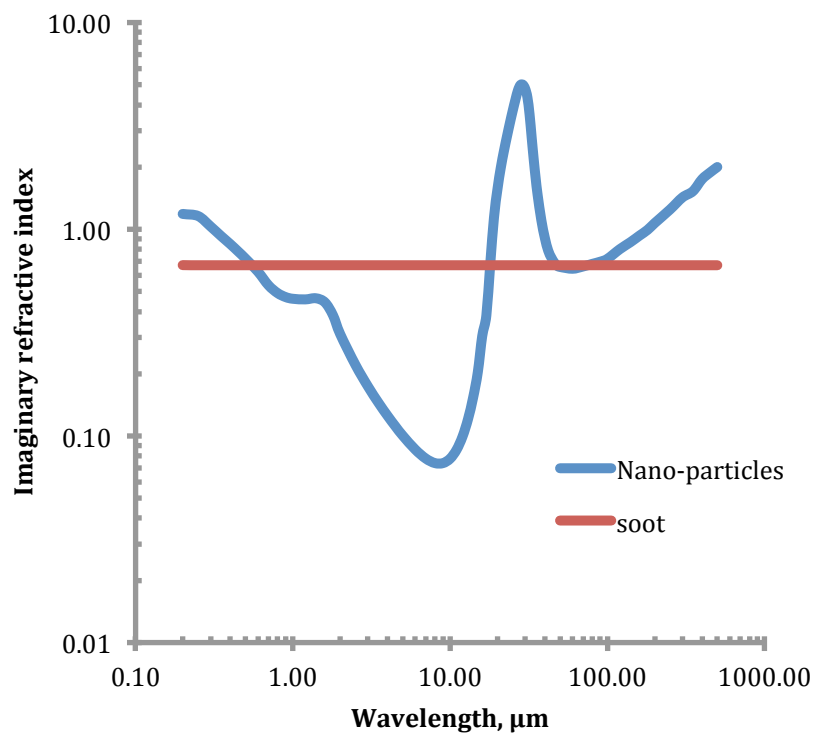


Fig. 3 The real and imaginary parts of the refractive index suggested for nano-particles, and for soot.